Clim. Past Discuss., 9, 6635–6682, 2013
www.clim-past-discuss.net/9/6635/2013/
doi:10.5194/cpd-9-6635-2013

Climate of the Past Discussions
Open Access

Orbitally tuned time scale and astronomical forcing in the middle Eocene to early Oligocene

T. Westerhold[1], U. Röhl[1], H. Pälike[1], R. Wilkens[2], P. A. Wilson[3], and G. Acton[4]

[1]MARUM – Center for Marine Environmental Sciences, University of Bremen, Leobener Strasse, 28359 Bremen, Germany
[2]Institute of Geophysics and Planetology, Univ. Hawaii, Honolulu, HI 96822, USA
[3]National Oceanography Centre Southampton, University of Southampton, Waterfront Campus, European Way, Southampton, SO14 3ZH, UK
[4]Department of Geography and Geology, Sam Houston State University, Huntsville, TX 77431, USA

Received: 12 November 2013 – Accepted: 2 December 2013 – Published: 18 December 2013

Correspondence to: T. Westerhold (twesterhold@marum.de)

Published by Copernicus Publications on behalf of the European Geosciences Union.

Abstract

Deciphering the driving mechanisms of Earth system processes, including the climate dynamics expressed as paleoceanographic events, requires a complete, continuous, and high-resolution stratigraphy that is very accurately dated. In this study, we construct a robust astronomically calibrated age model for the middle Eocene to early Oligocene interval (31–43 Ma) in order to permit more detailed study of the exceptional climatic events that occurred during this time, including the Middle Eocene Climate Optimum and the Eocene/Oligocene transition. A goal of this effort is to accurately date the middle Eocene to early Oligocene composite section cored during the Pacific Equatorial Age Transect (PEAT, IODP Exp. 320/321). The stratigraphic framework for the new time scale is based on the identification of the stable long eccentricity cycle in published and new high-resolution records encompassing bulk and benthic stable isotope, calibrated XRF core scanning, and magnetostratigraphic data from ODP Sites 171B-1052, 189-1172, 199-1218, and 207-1260 as well as IODP Sites 320-U1333, and -U1334 spanning magnetic polarity Chrons C12n to C20n. Subsequently we applied orbital tuning of the records to the La2011 orbital solution. The resulting new time scale revises and refines the existing orbitally tuned age model and the Geomagnetic Polarity Time Scale from 31 to 43 Ma. Our newly defined absolute age for the Eocene/Oligocene boundary validates the astronomical tuned age of 33.89 Ma identified at the Massignano (Italy) global stratotype section and point. Our compilation of geochemical records of climate-controlled variability in sedimentation through the middle-to-late Eocene and early Oligocene demonstrates strong power in the eccentricity band that is readily tuned to the latest astronomical solution. Obliquity driven cyclicity is only apparent during very long eccentricity cycle minima around 35.5, 38.3 and 40.1 Ma.

CPD
9, 6635–6682, 2013

1 Introduction

The Eocene/Oligocene transition (EOT) was a critical turning point in Earth's climatic history ~ 34 million years ago. The relatively ice-free warm world of the early Eocene shifted to one with lower greenhouse gas concentration and glacial conditions, accentuated by the growth of substantial ice sheets on Antarctica in the early Oligocene (Shackleton and Kennett, 1975; Grazzini and Oberhaensli, 1985; Pearson and Palmer, 2000; Zachos et al., 2001; Koeberl and Montanari, 2009). During this transition the carbonate compensation depth (CCD) deepened by ~ 1.2 km, marking one of the most pronounced perturbation during the past ~ 150 Myr (van Andel, 1975; Lyle et al., 2002; Pälike et al., 2012). The extremely close association between this CCD deepening event and rapid stepwise increase in the benthic oxygen stable isotope record indicates close coupling between carbon cycle perturbation and some combination of global cooling and growth in the Antarctic ice sheets (Coxall et al., 2005; DeConto et al., 2008; Lear et al., 2008; Liu et al., 2009; Bohaty et al., 2012). Yet the extent and stability of land ice in the "doubthouse" world (Prothero et al., 2003) of the middle and late Eocene remain uncertain (Prentice and Matthews, 1988; Ehrmann and Mackensen, 1992; Miller et al., 1991; Zachos et al., 1994, 1996; Edgar et al., 2007; Eldrett et al., 2007; Burgess et al., 2008). This interval in Earth's history is critical to testing climatic and evolutionary hypotheses about the deterioration of earlier Eocene conditions (Zachos et al., 2001).

Key records leading to recent breakthroughs in reconstructing the late Eocene and Oligocene epochs were those recovered during ODP Leg 199 (Lyle et al., 2002), at Site 1218 in particular (Fig. 1). Data from ODP Site 1218 permitted the development of an astronomical calibration of the entire Oligocene (Coxall et al., 2005; Wade and Pälike, 2004; Pälike et al., 2006), but low carbonate content in uppermost Eocene sediments at this site make detailed age control less certain than for the Oligocene. Although paleomagnetic age control for these time intervals is of high quality (e.g., Lanci et al., 2004, 2005), global stratigraphic correlation is hindered by lower mass accumulation rates,

CPD
9, 6635–6682, 2013

the absence of a detailed isotope stratigraphy, and sparser biostratigraphic control. To facilitate the development of an integrated magneto- and biostratigraphic framework with a stable isotope stratigraphy, IODP Expeditions 320/321 (Pacific Equatorial Age Transect – PEAT; Pälike et al., 2010) targeted the recovery of carbonate sections with a high quality magnetostratigraphy.

Decimeter-scale features in the sedimentary record as expressed in physical properties data from Leg 199 and Exp. 320/321 sites can be correlated over hundreds of kilometers at orbital resolution (Pälike et al., 2005; Westerhold et al., 2012a; Wilkens et al., 2013). Moreover, higher sedimentation rates and better preservation of carbonate especially in the middle to late Eocene of Exp. 320/321 sites (hereafter referred to as PEAT records) allows us to test and improve earlier efforts of astronomical calibrations for this time interval (e.g., Pälike et al., 2006) and further extend these back into the early to middle Eocene (Westerhold et al., 2012a). High-quality shipboard paleomagnetic records (Pälike et al., 2010), revised composite records, and detailed site-to-site correlation for all PEAT sites are available (Westerhold et al., 2012a; Wilkens et al., 2013) and are the prerequisite for further intercalibration of all major microfossil groups and refinement of magnetic polarity Chrons, particularly for the Eocene.

The main focus of our study is to establish a stratigraphic framework based on the identification of the stable long eccentricity cycle (405 kyr; Laskar et al., 2004; Hinnov and Hilgen, 2012) and subsequent detailed orbital tuning of the records. To this end we generated new geochemical records ($CaCO_3$, SiO_2, and Fe_2O_3 wt% obtained from calibrated XRF core scanning data; bulk stable isotope data) for Site 1218 and Sites U1333/U1334 spanning magnetic polarity Chrons C12n to C20n (31 to 43 Ma). In combination with published data we document the phase relationship of stable isotope data to XRF core scanning data, establish a stratigraphic framework for the Bartonian, Priabonian and early Rupelian Stages in the Equatorial Pacific and subsequently applied orbital tuning of the records. In this way, we provide a fully integrated and astronomically calibrated bio-, chemo-, and magnetostratigraphy for the Equatorial Pacific from 31 to 43 Ma.

CPD
9, 6635–6682, 2013

2 Material and methods

In addition to the new data from the PEAT records, we used and reinvestigated published data from Site 1052 (ODP Leg 171B – Blake Nose, Atlantic margin of northern Florida; Pälike et al., 2001), Hole 1172D (ODP Leg 189 – East Tasman Plateau; Röhl et al., 2004), and Site 1260 (ODP Leg 207 – Demerara Rise; Westerhold and Röhl, 2013). With respect to the depth scale we use "rmcd (revised CCSF-A)" for the revised composite core depth below seafloor at Site U1333 and U1334, and "rmcd" for revised meters composite depth at Site 1218 (for details on depth scale definitions see www.iodp.org/doc_download/3171-iodpdepthscaleterminologyv2 and Westerhold et al., 2012a).

2.1 XRF core scanner data

Sediments from Sites 1218, U1333 and U1334 were scanned using the XRF Core Scanner III (AVAATECH Serial No. 12) at the MARUM – University of Bremen (Röhl and Abrams, 2000; Röhl et al., 2007; Westerhold et al., 2007). Elemental intensities (Al through Fe) were collected every 2 cm down-core over a 1.2 cm^2 area with a down-core slit size of 10 mm using generator settings of 10 kV, a current of 0.12 mA, and a sampling time of 20 s at the split core surface of the archive half. The split core surface was covered with a 4-micron thin SPEXCerti Prep Ultralene1 foil to avoid contamination of the XRF measurement unit and desiccation of the sediment. Our data have been acquired by a Canberra X-PIPS Detector (Model SXP 5C-200-1500 V2) with 200 eV X-ray resolution, the Canberra Digital Spectrum Analyzer DAS 1000 and an Oxford Instruments 100W Neptune X-ray tube with rhodium (Rh) target material. Raw data spectra were processed by the Analysis of X-ray spectra by Iterative Least square software (WIN AXIL) package from Canberra Eurisys. For cores from the Site U1333 splice a higher energy run with 50 kV, a current of 1.0 mA, a Cu filter, and a sampling time of 30 s was added in order to also record Barium (Ba) intensity variations at 2 cm resolution.

CPD
9, 6635–6682, 2013

We scanned cores from the revised splice at each site (Westerhold et al., 2012a) with suitable overlaps to test the accuracy of the new composite section. Scanning was undertaken on archive halves from Site 1218 covering 201.68 to 293.20 rmcd, from Site U1333 covering 102.39 to 200.43 rmcd (m revised CCSF-A), and from Site U1334 covering 205.05 to 341.42 rmcd (m revised CCSF-A). Calcium (Ca) elemental intensity data have been transferred into carbonate wt% using $CaCO_3$ values analyzed on discrete samples for calibration purposes (Wilson et al., unpublished data). Fe and Si elemental intensity data have been quantified by calibrating normalized median-scaled (NMS, Lyle et al., 2012) XRF core scanning intensity data with ED-XRF analyses (Westerhold et al., unpublished). Calibrated high-resolution XRF core scanning intensities are calculated and reported as oxides (SiO_2, Fe_2O_3, $CaCO_3$), but for simplification we use Si, Fe, Ca in the text. Raw, NMS, and calibrated NMS XRF core scanning intensity data are reported in Supplement Tables S1–S4 (Site 1218, #5304 sample points), S5–S8 (U1333, #6835), and S9–S12 (U1334, #8102) (http://doi.pangaea.de/10.1594/PANGAEA.821903).

2.2 Bulk stable isotope data

Stable isotope measurements on 1369 powdered (freeze-dried) bulk sediment samples from Sites U1333 and U1334 were performed on a Finnigan MAT 251 mass spectrometer equipped with an automated carbonate preparation line at MARUM, University Bremen. The carbonate was reacted with orthophosphoric acid at 75°C. Analytical precision based on replicate analyses of an in-house standard (Solnhofer Limestone) averages 0.05‰ (1s) for $\delta^{13}C$. All data are reported against VPDB after calibration of the in-house standard with NBS-19. In detail, we processed 461 samples from Site U1333 spanning the interval C15n to C17n.1n (138.71–152.14 rmcd (m revised CCSF-A)) and 908 samples from Site U1334 spanning the interval C16n.2n to C18n.1n (314.59–341.44 rmcd (m revised CCSF-A)). Bulk stable isotope data for U1333 and U1334 are reported in Tables S13 and S14, respectively http://doi.pangaea.de/10.1594/PANGAEA.821903.

CPD
9, 6635–6682, 2013

2.3 Paleomagnetic data Site U1333

The magnetostratigraphy for Site U1333 was originally constructed from continuous paleomagnetic measurements made every 5 cm along the archive-half sections of all cores collected with the Advanced Piston Corer (APC) during Expedition 320 (Pälike et al., 2010). Magnetic cleaning typically was limited to alternating field (AF) demagnetization in peak fields of 20 mT, which was shown to be sufficient to remove drilling-related magnetic overprints and to resolve a primary depositional remanence magnetization (Pälike et al., 2010).

To determine the paleomagnetic direction more accurately and the depths of magnetic reversal boundaries more precisely, while also providing relative paleointensity estimates and environmental magnetic records, 169 U-channel samples (2 cm × 2 cm × 150 cm) were collected continuously along the spliced composite stratigraphic section from 0 to 190 rmcd. Paleomagnetic results from the lower 88 U-channel samples (96–190 rmcd), which provide a magnetostratigraphy that spans from the middle of Chron C11r to within Chron C20n, are presented here. Results for the upper 81 U-channel samples (0–96 rmcd), spanning from the base of Chron C6n to the middle of Chron C11r, are presented in Guidry et al. (2013).

For the interval from 96–190 rmcd, each U-channel sample was subjected to progressive AF demagnetization from 0 mT up to 80 or 100 mT typically in 8 to 11 steps and the magnetic remanence was measured every 1 cm following each step. Paleomagnetic directions were determined from principal component analysis (PCA) in which remanence measurements from at least five demagnetization steps for each interval were fit to lines (Kirschvink, 1980). Linear fits were well constrained, with average maximum angular deviation (MAD) angles of 2.3° for the 10 896 intervals used in the magnetostratigraphic interpretation (Supplement Fig. S12 and Tables S17–S19). The revised magnetostratigraphy is derived from the distinct ~ 180° alternations in magnetic declination that occur along the composite stratigraphic section (Supplement Fig. S13 and Tables S17–S19). Overall, the revised magnetostratigraphy differs very little from

CPD
9, 6635–6682, 2013

that obtained during Expedition 320 (Supplement Fig. S13); most magnetozone boundaries were adjusted by < 5 cm, with adjustments > 50 cm for only 3 of the 23 reversals between Magnetozones C11r and C20n (Supplement document 1). This attests to the stability of the primary magnetization of these sediments. Other details of the measurements, processing, and results are provided in Supplement document 1, with raw paleomagnetic data and the PCA paleomagnetic directions for the three holes given in Supplement Tables Ss17–S19.

3 Results

The sediments studied consist of nannofossil ooze or chalk, radiolarite, and claystone (Pälike et al., 2010) and therefore varying amounts of carbonate, opal, and terrigenous material. Calibrated high-resolution XRF core scanning intensities show highly dynamic wt% values in late Eocene sediments and lower amplitude variations in middle Eocene (middle of Chron C18r to C19n) and very early Oligocene (younger than Chron C13r) nannofossil chalks and oozes with $CaCO_3$ contents averaging around 75 to 80 wt% (Fig. 2). The lower amplitude variations correspond to intervals when the CCD was relatively deep in the equatorial Pacific (Lyle et al., 2005; Pälike et al., 2012). Carbonate content drops to near zero at all sites across the C18r/C18n boundary during the peak of the Middle Eocene Climate Optimum (MECO; Bohaty et al., 2003) and within Chron C15r. Variations in both XRF-derived Si and Fe are anti-correlated to the Ca content except for the MECO interval across the C18n2n/C18r boundary at Site 1218. Fe mainly comes from terrigenous material, whereas the Si signal probably represents a mixture of radiolarian ooze with terrigenous clay. The shallowest Site U1334 contains the highest carbonate content of all PEAT records, but also contains more iron oxide than the other sites because of the relatively higher clay content (Pälike et al., 2010). In contrast, Sites 1218 and U1333 reveal a greater amount of Si averaging 40–45 wt% in the late Eocene, dropping to ~ 20 wt% at the EOT. The amplitude in sediment composition variations of all elements (or calculated oxides) increase simultaneously

CPD
9, 6635–6682, 2013

at all sites close to the Chron C17r/C18n boundary, are especially pronounced at Site U1334 from the middle of Chron C16n through Chron C13r, and decrease dramatically in two steps across the EOT (Fig. 2) akin to behavior documented in the published record from Site 1218 (Coxall et al., 2005).

The bulk carbon stable isotope data (black curves in Fig. 2) show long-term increases from the top of Chron C18n.1n to C15n, a subsequent strong decrease up to the upper Chron C13r, and the well-known stepped increase across the EOT (Coxall et al., 2005). Pronounced higher frequency variations are related to short (100 kyr) and long (405 kyr) eccentricity cycles as also observed in a latest Eocene to Oligocene benthic isotope record from Site 1218 (Pälike et al., 2006).

The phase relation between bulk carbon isotopes and XRF data is not persistent over the studied interval (see next section) complicating the tuning process. Lower carbon isotope values correspond to higher carbonate, lower Si and lower Fe contents from the middle of Chron C18r to C15n. For the interval younger than Chron C15n lighter carbon isotope data correspond to lower carbonate, higher Si and higher Fe. This phase relation, although based on relatively lower-resolution stable isotope data, most likely is also present during the interval with high carbonate content from the middle of Chron C18r to the base of Chron C19n. To establish a cyclostratigraphy we assume that the phase relation between bulk and benthic stable isotopes and eccentricity to be constant over time. Based on results from other Paleogene successions (Lourens et al., 2005; Pälike et al., 2006; Zachos et al., 2010; Westerhold et al., 2011) we assume that lighter carbon isotope data in the Milankovitch frequency range (95 and 405 kyr) correspond to eccentricity maxima.

4 Cyclostratigraphic framework

Constructing a cyclostratigraphy in late Eocene sediments is quite challenging because relatively strong changes in the CCD and accumulation rates indicates a highly dynamic environment between ~ 39 Ma and ~ 33 Ma (Moore and Kamikuri, 2012; Pälike

CPD
9, 6635–6682, 2013

et al., 2010, 2012). Reworking of radiolarians at Sites 1218 and U1333 in the interval from Chron C17r to the EOT poses an additional problem (Moore, 2013), however Site U1334 provides a reliable record because it is much less affected by reworking then the other two sites. Our initial goal is to identify the long eccentricity cycle in our data series and undertake a basic orbital tuning to the La2011 eccentricity solution. To aid inspection of the proposed correlation to the La2011 solution we count the long and short eccentricity cycles and apply a numbering scheme (see Supplement Fig. 8). The numbering scheme for the long eccentricity cycles (405 kyr) follows the approach of Wade and Pälike (2004) where eccentricity maxima are counted back in time (see Hinnov and Hilgen, 2012). The short eccentricity cycle (100 kyr) count numbers are defined as positive numbers in the Oligocene and negative numbers in the Eocene with the Eocene/Oligocene boundary defined as the starting point. Highly variable sedimentation rates mean that it is not a straightforward task to assign the short eccentricity cycle across all sites and throughout the sections. However, the integrative approach of considering three sites with multiple data records at least allows correlation of cyclostratigraphic interpretations between sites. Time-series analysis was applied as in Westerhold and Röhl (2009). Evolutionary wavelet power spectra (Wavelet software was provided by C. Torrence and G. Compo http://paos.colorado.edu/research/wavelets) were computed for the bulk stable δ^{13}C data from Sites U1333 and U1334 (Supplement Fig. S1), and the calibrated Si, Fe, and Ca XRF core scanning data from Sites 1218, U1333, and U1334. All records are analyzed in the depth domain, and in the time domain only using magnetostratigraphy (Supplement Table S16). Due to the prominent change in lithology and accumulation rate at the EOT we calculate wavelet power spectra for the Oligocene (Supplement Figs. S2–S4) and the Eocene intervals (Supplement Figs. S5–S7) separately. For clarity of presentation we divided the time series into four intervals.

CPD
9, 6635–6682, 2013

4.1 Chron C12r to C13n – early Rupelian

The cyclostratigraphy of the carbonate-rich interval from the base of Chron C12n to the base of Chron C13n was previously constrained by the 405 kyr cycles in the benthic stable isotope record from Site 1218 (Coxall et al., 2005; Wade and Pälike, 2004; Pälike et al., 2006; Coxall and Wilson, 2011) (Fig. 3). Improvements in the composite section (Westerhold et al., 2012a, Supplement Fig. S9) in this interval permit us to re-tune the Site 1218 records resulting in smoother sedimentation rates than originally published (Pälike et al., 2006). The 405 kyr cycle is apparent in the Site 1218 benthic δ^{13}C record with a period of ∼ 6 m, in Site U1334 Si data with a period of ∼ 7 m, and in Site U1333 Si data with a period of ∼ 5 m (Fig. 3; Supplement Fig. S2). These periods can also be observed in the Ca record (Supplement Fig. S3). Low Fe contents mean that cyclicity is less visible in the Fe records (Fig. 3) at sites 1218 and U1333 than at Site U1334. Long and short eccentricity minima (lighter values) in benthic and bulk δ^{13}C correspond to Si and Fe maxima. Based on the pattern comparison between the La2011 solution and the benthic δ^{13}C record from Site 1218 we arrive at the same correlation of the stable 405 kyr cycle as Pälike et al. (2006) with Chron C12r and C13n spanning cycles 78 to 83. The short eccentricity cycles are clearly present in the lower part of Chron C12r and the upper part of Chron C13n, where amplitudes in Si and Ca data are more pronounced. In the upper part of Chron C12r these cycle are present but less evident. We have tentatively identified these short eccentricity cycles and correlated them to La2011 (green numbers in Fig. 3). Four ash layers can be traced at all three sites and were used as independent correlation features (Kuroda and Westerhold, 2013) to further guide our correlation.

4.2 Chron C13n to C15r – Eocene/Oligocene Transition (EOT)

The three sites investigated (Fig. 4) allow a basic cyclostratigraphy from the base of Chron C13n to the base of Chron C15r, which covers the long eccentricity cycles 84 to 88, with the EOT spanning cycles 84 to 85. The stable 405 kyr cycle is readily identified

CPD
9, 6635–6682, 2013

in the Si data at Site U1334 with a period of ~ 3 m, at Site 1218 with a period of ~ 2.4 m, and at Site U1333 with a period of ~ 1.2 m (Fig. 4; Supplement Fig. S5). Bulk stable carbon isotope data also reveal a strong 405 kyr component (Supplement Fig. S1) but not for the interval equivalent to the long eccentricity cycles 85 to 86 where bulk carbon isotope data demonstrate marked site-to-site consistency but no orbital structure and are therefore not suitable for tuning. An option we chose to follow to alleviate this challenge is to use the Si data from Site U1334 to identify the long eccentricity cycles because the phase relationship (lower δ^{13}C corresponds to Si maxima) seems consistent on the run up to this interval (Fig. 4).

4.3 Chron C15n to C17r – middle Priabonian to late Bartonian

The combination of records from three equatorial Pacific sites (Fig. 5) with the ODP Site 1052 section (Fig. 6, Pälike et al., 2001) allows definition of a cyclostratigraphic framework for Chrons C15n through C17r (covering long eccentricity cycles 88 to 95). In this interval the bulk δ^{13}C and Si data from Sites U1333 and U1334 best resolve the 405 kyr cyclicity. Site 1218, however, suffers from an overall lower sedimentation rate in combination with strong carbonate dissolution notably around 250 rmcd, long eccentricity cycle 85 (Fig. 5). Both sites, 1218 and U1333, exhibit prominent fluctuations in Si, Ca, and Fe values due to frequent and substantial CCD changes. In contrast, the shallower Site U1334 contains on average 70 wt% carbonate from Chron C17r up to C16n.2n. Carbonate dissolution accompanied by elevated Si and Fe values also occurs at all sites around the Chron C16n/C15r boundary (eccentricity cycle 85). The long eccentricity cycle can be clearly assigned in the bulk δ^{13}C data from Sites U1333 and U1334 with a period of ~ 2.3 m and ~ 3.8 m, respectively (Fig. 5, S1). In this time interval the long eccentricity-related lower values in bulk δ^{13}C correspond to Si and Fe minima and Ca maxima (Fig. 5). The cyclostratigraphy based on the δ^{13}C data from Sites U1334 and U1333 is consistent with the extracted cyclicity in the Fe record from Site 1218. At Site U1334 a shift in phase relation occurs at 317 rmcd (m revised CCSF-A) close to the base of C16n.2n. This shift is not observed at Sites U1333 and 1218,

CPD
9, 6635–6682, 2013

which indicates that the cyclostratigraphy for Chron C16 may remain indistinct. Fortunately, the record from ODP Site 1052 (Pälike et al., 2001; Fig. 6) also captures Chrons C16 and C17 with well expressed eccentricity-modulated precession cycles (except for a ~ 600 kyr period in the upper part of Chron C16n with obliquity dominance). The long eccentricity cycle at Site 1052 encompasses ~ 11 m intervals in the Ca/Fe XRF core scanning data. The obliquity-dominated interval in C16 (Pälike et al., 2001) lies within cycle 88 and upper cycle 89.

In both the La2010 and La2011 solutions, the long eccentricity cycle 88 is one of the prominent very long eccentricity (2.4 myr) nodes with very low amplitude modulation of eccentricity. The orbital configuration of low eccentricity in combination with observed high obliquity amplitudes in the data has also been observed in early Eocene records (Westerhold and Röhl, 2009) and could be an indication of the increased influence of high-latitude processes on low latitude deep ocean chemistry during minima in the very-long eccentricity cycle. Furthermore, our integration of the cyclostratigraphic results suggests that Chron C16n.1n is definitely located within cycle 88.

4.4 Chron C17r to C20n – Bartonian to late Lutetian

To establish a reliable cyclostratigraphy for equatorial Pacific sites covering Chron C17r through C20n we integrated data from Sites 1218 and U1333 with records from Site 1260 (ODP Leg 207, Demerara Rise; Westerhold and Röhl, 2013) and Hole 1172D cyclostratigraphies (ODP Leg 189, East Tasman Plateau, Röhl et al., 2004) (Fig. 7). This step is needed because of strong dissolution during the MECO (Bohaty and Zachos, 2003) interval (~ 170 rmcd in the Site U1333 record and ~ 273 rmcd in the Site 1218 section) at both PEAT sites, the lack of high quality/high-resolution stable isotope data for the entire interval, and pronounced changes in sedimentation rate between the short eccentricity cycle −70 and −69.

At Sites 1260 and 1172, the ~ 10 m long eccentricity cycles can be extracted from benthic isotope data (Edgar et al., 2007) and XRF core scanning Ca/Fe data (Röhl et al., 2004). This provides a solid framework for Chron C18 and C19 spanning long

CPD
9, 6635–6682, 2013

eccentricity cycles 96 to 105 (Supplement Fig. S8). At Sites 1218 and U1333 the long eccentricity cycle can be identified in Si and Fe data as far as Chron C18n.1r with a length of ~ 2.4 m and ~ 2.8 m, respectively (Fig. 7, Supplement Figs. S5 and S6). The sparse stable isotope data available for this interval still suggest that the phase relation to Si, Fe, and Ca is the same as in the previously discussed interval. Thus, for the interval from short eccentricity cycle −45 to −69 we assumed the same phase relation and tried to identify the 405 kyr cycles by correlating the equatorial Pacific records to those from Sites 1260 and 1172. At Site 1218 the sedimentation rates drop from ~ 1.5 to ~ 0.5 cm kyr^{-1} and at Site U1333 from ~ 1.0 to ~ 0.5 cm kyr^{-1} (Supplement Fig. S10) during short eccentricity cycle −70 leading into the MECO. According to depth backtracking Site 1218 (3152 m b.s.l.) was almost 400 m shallower than Site U1333 (3533 m b.s.l.) during the top of Chron C19n (Pälike et al., 2010), which may explain why the sedimentation rate at Site 1218 is much higher than at Site U1333. Our correlation suggests that the 405 kyr cycle in the Site 1218 record has a length of ~ 9.1 m starting at C19n to short eccentricity cycle −70, and ~ 4.5 m from there up to the top of C18n.2n (Fig. 7). At Site U1333 the 405 kyr cycle has a length of ~ 2.7 m and ~ 4.0 m in the respective intervals. This implies an increase in sedimentation rates at Site U1333 during the MECO that is not visible in the Site 1218 record. However, the MECO interval was only cored in a single hole at Site U1333 (Westerhold et al., 2012a). The high sedimentation rates could be an artifact if the upper part of Core U1333A-18X covering the MECO was artificially stretched by coring.

In order to compare the geological data with orbital solutions and subsequently anchor the floating 405 kyr stratigraphic framework in absolute time by orbital tuning, the observation of a dominant obliquity component in Hole 1172D (Röhl et al., 2004) during long eccentricity cycles 95 and 96 as well as between cycle 99 and 100 (Fig. 7) is very important. As observed in the early to middle Eocene at ODP Site 1258 (Westerhold and Röhl, 2009) an orbital configuration of low eccentricity in combination with high obliquity amplitudes during very long eccentricity minima could have fostered the development of obliquity-dominated intervals. Therefore, the dominant obliquity component

CPD
9, 6635–6682, 2013

intervals in 1172D can help to identify the position of very long eccentricity cycle minima in the geological data and are very important features for evaluating the accuracy of orbital solutions for eccentricity.

5 Astronomical tuning

Astronomical tuning, the correlation of cyclic variations in the geological record to astronomical computations of solar insolation on Earth, depends on the accuracy of the orbital target curves and the completeness of the geological dataset to be calibrated. Because of uncertainties in radioisotopic dating (Westerhold et al., 2012b) and limits of astronomical calculations (Laskar et al., 2004, 2011a, b) we first developed an independent stratigraphic framework based on the identification of the stable long eccentricity cycle. Subsequently, we tuned the geological data of Sites 1218, U1333 and U1334 to the La2011 orbital solution for Earth's eccentricity starting in the early Oligocene, which has been anchored to the Astronomically Tuned Neogene Time Scale (Lourens et al., 2005; Pälike et al., 2006).

The strength of obliquity cycles in the Ca/Fe data series from Site 1052 (Pälike et al., 2001) (Fig. 6) in Hole 1172D (Röhl et al., 2004) (Fig. 7) during minima in the very long eccentricity at 35.4 (cycle 88) and 38.2 (cycle 95) Ma suggests that orbital solutions and geological data are consistent with one another for this time interval. For consistency in orbital tuning procedures we used an ETP target curve as described in Pälike et al. (2006), although we applied the La2011 eccentricity and the La2004 values for precession and obliquity. Basically, the La2011 and La2004 eccentricity solutions are almost identical up to 42 Ma with only very minor deviations in the very long eccentricity minima (Westerhold et al., 2012b). Currently there is no precession and obliquity target available based on La2011, thus we chose to combine the available curves. To achieve a consistent age model between all sites we utilized all available information and defined age tie points for each site separately. This way we developed an accurate astronomically calibrated time scale for the middle Eocene to early Oligocene

CPD
9, 6635–6682, 2013

(31–43 Ma) interval for the PEAT sites and Site 1218 (age tie points are given in Supplement Table S15). Sedimentation rates based on the astronomical calibration are relatively smooth (Fig. 8). New age estimates and durations for the Geomagnetic Polarity Time Scale are presented in Tables 1 and 2 (detailed PEAT magnetostratigraphy in Supplement Table S16) and discussed below.

6 Discussion

Absolute age calibration of the middle to late Eocene interval is not a straightforward matter because of the uncertainties in the exact position of ash layers with respect to magnetostratigraphy in continental sections, the uncertainty in radioisotopic dating, and the sparse coverage with high-quality carbonate rich deep sea drill cores (see detailed discussion in Hilgen and Kuiper, 2009; Vandenberghe et al., 2012; Westerhold et al., 2012b). Here, our focus is the construction of a cyclostratigraphic framework based on the identification of the stable long eccentricity cycle (405 kyr) in deep-sea records for the middle Eocene to early Oligocene (31–43 Ma).

6.1 Duration of magnetochrons and comparison to standard geomagnetic polarity time scales

Our new stratigraphic framework provides estimates of the absolute ages of magnetic polarity Chrons C12r to C20n and their positions in the 405 kyr cycle number scheme. Based on our multiple site approach we can be confident that our data set is stratigraphically complete to the long eccentricity cycle level. Astronomically tuning to the La2011 orbital solution allows us to refine age estimates down to the 100 kyr level. We consider the ages of magnetochron boundaries to be as accurate; only for Chron C15n and the top of C16n.1n does some uncertainty still exist.

In the early Oligocene interval, comparison of our new ages with published GPTS ages (Fig. 9, Table 1) shows that our ages are very close to those derived from previous

CPD
9, 6635–6682, 2013

orbital tuning of Site 1218 (Pälike et al., 2006) down to the E/O boundary. However, our new astronomically tuned absolute age for the Eocene/Oligocene boundary (Chron C13r.14) is 33.89 Ma, which is ~ 100 kyr older than the age in Pälike et al. (2006), and thus validates the astronomical tuned age from the Massignano (Italy) global stratotype section and point (GSSP) (Brown et al., 2009).

In the middle to late Eocene interval down to Chron C18r, our ages are close to the ages of Cande and Kent (1995, CK95) and Pälike et al. (2006) but are about 300 kyr younger than the ages given by GPTS2012 (Ogg, 2012; Vandenberghe et al., 2012) for all reversals from the base of Chron C15r to the base of Chron C17r. Figure 9 shows that GPTS2004 has younger and much shorter durations of magnetochrons between 35 and 41 Ma than the other timescales. The GPTS2004 compresses the middle to late Eocene chrons because it uses a relatively young age of 45.60 ± 0.38 Ma for an ash layer in C21n compared to CK95 (for discussion see Westerhold and Röhl, 2009) and GPTS2012.

The most obvious differences in the age estimates are observed in the late Eocene, namely for Chron C15 and the younger part of Chron C16. Our new GPTS as well as Pälike et al. (2006) gives durations for both Chrons C15r and C16n.1r that are shorter than other time scales and gives durations for Chron C13r that are longer than other time scales. Pälike et al. (2012) suggested this was related to highly dynamic variations in the CCD in the equatorial Pacific. Other suitable sites with sufficient high-quality magneto- and cyclostratigraphy to decipher this part of the time scale fully are not yet available from the deep sea. Two marine sections and one continental section with established magneto- and cyclostratigraphies are, however, already available for Chron C13r: the Solent Group from the Isle of Wight in the UK (Gale et al., 2006), the Massignano GSSP section in central Italy (Premoli Silva and Jenkins, 1993; Jovane et al., 2006; Brown et al., 2009), and the lacustrine records from the Xining Basin on the Tibetan Plateau (Dupont-Nivet et al., 2007; Xiao et al., 2010). Both the Solent Group record (Gale et al., 2006) and the Massignano section (Jovane et al., 2006; Brown et al., 2009) suggest that Chron C13r lasted the equivalent of 2.5 long eccentricity

CPD
9, 6635–6682, 2013

cycles or ∼ 1000 kyr. Obliquity-driven cyclicity in physical properties from the Xining basin record imply an even shorter duration, on the order of 800 to 900 kyr, of Chron C13r (Xiao et al., 2010). This would require that PEAT records overestimate the duration of Chron C13r by ∼ 400 kyr or one long eccentricity cycle. Alternatively, the Solent Group record may be condensed or incomplete in C13n and around the C13r/C15n boundary. A hint for this scenario could be a hiatus in Chron C13n and the fact that the Chron C13r/C15n boundary is characterized only by an incomplete illitic clay cycle.

At the Massignano section uncertainties may lie in the array of estimated 10–12 m length for Chron C13r (Lowrie and Lanci, 1994). Based on average sedimentation rates of 0.7 cm kyr^{-1} the dominant cycles in the Massignano section with lengths of 32, 72 and 284 cm relate to periods of 45, 102 and 405 kyr, respectively (Jovane et al., 2006). These periods and their frequency ratio are diagnostic of obliquity and eccentricity related cycles. However, this basic calculation does not account for the range in thickness of Chron C13r (10 to 12 m). Applying our estimate of 1376 kyr for the duration of Chron C13r (Table 2), sedimentation rates at Massignano would then range between 0.73 cm kyr^{-1} (10 m thickness of Chron C13r) and 0.87 cm kyr^{-1} (12 m thickness of Chron C13r). The cyclicity in the Massignano section and our 1376 kyr duration for Chron C13r are most consistent with the 10 m estimate of thickness for Chron C13r in the Massignano section. But a duration of 1376 kyr for C13r is not consistent with the interpretation that lacustrine records from the Xining Basin (Xiao et al., 2010) are obliquity driven. Chron C15n and C15r are shorter in the PEAT records than estimated for the Massignano section (Jovane et al., 2006; Brown et al., 2009). Sedimentation rates increase during Chrons C15 and C16 in the PEAT record (Fig. 8). In the carbonate record of interval C16n.1n to early Chron C13r at Massignano a temporary shift from obliquity to 26–30 kyr cycles occurs and is interpreted as a possible feedback to impact/comet shower related climate change (Brown et al., 2009). If we apply our calculated sedimentation rates of ∼ 0.8 cm kyr^{-1}, however, the observed 26–30 kyr cycles in the interval from 5.6 to 13 m at Massignano (Brown et al., 2009) becomes ∼ 20 kyr cycles. Although the thickness of Chron C15r in the Massignano section is not

CPD
9, 6635–6682, 2013

unambiguous (see Lowrie and Lanci, 1994), this interpretation indicates that the duration of Chron C15r should be about a third shorter than the 383 kyr of Jovane et al., (2006). If correct, the duration of C15r is ∼ 250 kyr – as observed at the PEAT sites (214–286 kyr). The 74 kyr estimate of Pälike et al. (2006) is far too short (also see discussion in Westerhold et al., 2012a) as indicated by the unusual sedimentation rate increase in C15 (Supplement Fig. S10). The durations for Chron C16n.1n and C16n.1r are not as well resolved in the PEAT record as in other records studied.

Ages and durations of magnetochrons Chron C16n.2n through C17n.3r are well constrained by a combination of the PEAT records and Site 1052 results. Due to the coarser sampling interval the error for the magnetic reversal boundaries obtained from Site 1052 is relatively large. Pälike et al. (2001) used the La1993 (Laskar et al., 1993) solution for orbital calibration and therefore the tuned ages for Site 1052 differ by ∼ 100 kyr compared to those applying the now available La2011 solution. Our new estimates are close to CK95 and Pälike et al. (2006) ages, but older than GPTS2004 and younger than GPTS2012. For Chrons C18 and C19, integration of the PEAT records with records containing well-pronounced cyclicity from Sites 1172 and 1260 allows a very accurate age calibration from Chron C18 to the top of Chron C20n. The ages from CK95 become increasingly older and those from GPTS2004 increasingly younger in this interval from these two sites. The difference originates from a relatively old (young) age for the ash in C21n.33 of 46.8 Ma (45.6 Ma) in CK95 (GPTS2004). Therefore, the GPTS2012 calibration omitted this tie point and alternatively used the $^{40}Ar/^{39}Ar$ age of 43.35 ± 0.5 Ma for the Mission Valley Ash (California, USA) near the base of C20n (Prothero and Emry, 1996; Walsh et al., 1996; Smith et al., 2010) (Fig. 9). According to our tuned GPTS ages the age of the Mission Valley Ash date is about 300 kyr too old. One explanation could be that the GPTS2012 applied an age of 28.201 Ma (Kuiper et al., 2008) for the FCT $^{40}Ar/^{39}Ar$ dating standard.

CPD
9, 6635–6682, 2013

6.2 Paleoceanographic implications

Two prominent features in the PEAT records and our astronomical time scale need to be briefly discussed. One is the change in phase relationship between stable carbon isotope and XRF core scanning data in relation to the short and long eccentricity cycle (see Fig. 10 and Supplement Fig. S11). From 43 Ma, where our study starts, to 40.5 Ma the records are in-phase with low Fe and Si, and with high Ca corresponding to lower $\delta^{13}C$ values. The phase relation switches around 40.5 Ma to an anti-phase mode at all three sites and this pattern remains until ~ 36 Ma. Due to strong dissolution no distinct relation is observable between 36–35 Ma. After ~ 35 Ma the records are again in phase. The switch in phase relation of isotopes vs. carbonate content is similar to the shift from the Atlantic-type (high carbonate in interglacials) to Pacific-type (high carbonate in glacials) carbonate stratigraphy observed during the earliest Gauss Magnetic Chron (3.18–3.41 Ma) in equatorial Pacific sediments (Moore et al., 1982; Dunn, 1982), close to the onset of Northern Hemisphere glaciation. The shift in phase relation prior to the EOT could be related to a change in the deep and intermediate water circulation (Katz et al., 2011). This reorganization in ocean circulation is also expressed in the response of the equatorial Pacific to orbital forcing and probably also affected the distribution of nutrients.

The other important feature is the occurrence of an obliquity-dominated cyclicity coinciding with the very long eccentricity minima at 35.5 Ma (Site 1052 (Pälike et al., 2001), Fig. 6, 405 cycle 88), at 38.3 Ma and 40.1 Ma (both Site 1172, Fig. 7, cycles 95 and 99/100). Prominent obliquity cycles are not present in the PEAT records probably due to their low latitude setting. At both intervals around 40.1 and 38.3 Ma relatively high amounts of ice-rafted debris (IRD) have been reported from the Greenland Sea Site 913 (Eldrett et al., 2007; Tripati et al., 2008) with an age model approach based on CK95, which is therefore chronologically comparable to the PEAT record. At 35.5 Ma an increase in IRD is reported from the same high latitude site (Eldrett et al., 2007) in Chron C15r, coincident with a cooling shift observed at the Southern Ocean Site 689B

CPD
9, 6635–6682, 2013

(Vonhof et al., 2000) and a major sea level fall (Peters et al., 2010). From our new stratigraphic framework defined for the PEAT record, we would hypothesize that the cooling as reflected by the higher amount of IRD in the Greenland Sea might be fostered by the very long eccentricity minima at 35.5 Ma, 38.3 Ma and 40.1 Ma (405 kyr cycles 88, 95, and 100). The occurrence of contemporaneous obliquity cycles at Sites 1172 and 1052 suggests that to some extent high-latitude processes driven by orbital obliquity strongly influenced ocean circulation during very long eccentricity minima. Temperatures at high latitudes cool enough to form ice in the Arctic already occurred at 47–46 Ma ago (Stickley et al., 2009; St. John et al., 2008). With decreasing atmospheric CO_2 (Peason and Palmer, 2000; DeConto and Pollard, 2003; Pollard and DeConto, 2005) in an environment and aftermath of gateway evolution (Bijl et al., 2013), orbital forcing might have fostered ephemeral ice buildup at the poles subsequently causing a sea level fall (Peters et al., 2010). The data presented here from PEAT so far support the suggestion that high-latitude processes had little effect in equatorial regions (Pearson et al., 2007) during the late Eocene.

7 Summary and conclusions

We have assembled a new stratigraphic framework based on the identification of the stable long eccentricity cycle for the middle to late Eocene into the early Oligocene (43 to 31 Ma) across the Eocene/Oligocene Transition. Our cyclostratigraphies are based on integrated high-resolution bulk and benthic stable isotope data, calibrated XRF core scanning data and magnetostratigraphy from Pacific Equatorial Sites 1218 (ODP Leg 199), U1333, U1334 (IODP Expeditions 320/321), Atlantic Sites 1052 (ODP Leg 171) and 1260 (ODP Leg 207) as well as Tasman Sea Site 1172 (ODP Leg 189). We tune the records to the La20011 orbital solution to establish a robust absolute age model. Our chronology provides new accurate estimates for the Geomagnetic Polarity Time Scale (GPTS) covering Chrons C12n to C20n that are calibrated to the short eccentricity cycle level. However, for now the age model is still ambiguous for Chron C15n to the

CPD
9, 6635–6682, 2013

top of C16n due to the highly dynamic variability of the Carbonate Compensation Depth in the equatorial Pacific and pending coverage of this interval with high-resolution stable isotope data. The age estimates support the CK95 calibration, are discordant with the GPTS2004 calibration, and reveal a systematic offset of about +300 kyr relative to GPTS2012 for late Eocene reversals from Chron C15r to C17r. The chronology of changes in the phase relationship in PEAT records between XRF core scanning data and stable carbon isotope data suggests a close linkage to changes in overall deep-ocean circulation at 40.5 and 35–36 Ma. The synopsis of the records utilized for the cyclostratigraphy reveals strong obliquity related cycles in mid to high-latitude sites (1052, 1171) during very long (2.4 myr) eccentricity minima at 35.5, 38.3 and 40.1 Ma.

Supplementary material related to this article is available online at http://www.clim-past-discuss.net/9/6635/2013/cpd-9-6635-2013-supplement.pdf.

Acknowledgements. This research used samples and/or data provided by the Ocean Drilling Program (ODP) and Integrated Ocean Drilling Program (IODP). Data have been acquired in the XRF Core Scanner Lab at the MARUM – Center for Marine Environmental Sciences, University of Bremen, Germany. We thank Monika Segl and her team (MARUM) for stable isotope analysis. Funding for this research was provided by the Deutsche Forschungsgemeinschaft (DFG), NERC, and the National Science Foundation (Grant NSF OCE-0961412). We are indebted to V. Lukies (MARUM) for assisting in XRF core scanning, and the staff at BCR and GCR for core handling. The complete data set presented in this paper is available online in the WDC-MARE PANGAEA database under www.pangaea.de.

References

Bijl, P. K., Bendle, J. A. P., Bohaty, S. M., Pross, J., Schouten, S., Tauxe, L., Stickley, C. E., McKay, R. M., Röhl, U., Olney, M., Sluijs, A., Escutia, C., Brinkhuis, H., and Scientists, E.:

Eocene cooling linked to early flow across the Tasmanian Gateway, P. Natl. Acad. Sci. USA, 110, 9645–9650, doi:10.1073/pnas.1220872110, 2013.
Bohaty, S. and Zachos, J. C.: Significant Southern Ocean warming event in the late middle Eocene, Geology, 31, 1017–1020, 2003.
Bohaty, S. M., Zachos, J. C., Florindo, F., and Delaney, M. L.: Coupled greenhouse warming and deep-sea acidification in the middle Eocene, Paleoceanography, 24, PA2207, doi:10.1029/2008pa001676, 2009.
Bohaty, S. M., Zachos, J. C., and Delaney, M. L.: Foraminiferal Mg/Ca evidence for Southern Ocean cooling across the Eocene–Oligocene transition, Earth Planet. Sc. Lett., 317–318, 251–261, doi:10.1016/j.epsl.2011.11.037, 2012.
Brown, R. E., Koeberl, C., Montanari, A., and Bice, D. M.: Evidence for a change in Milankovitch forcing caused by extraterrestrial events at Massignano, Italy, Eocene–Oligocene boundary GSSP, in: The Late Eocene Earth – Hothouse, Icehouse and Impacts, edited by: Koeberl, C. and Montanari, A., Geol. S. Am. S., 452, 119–137, doi:10.1130/2009.2452(08), 2009.
Burgess, C. E., Pearson, P. N., Lear, C. H., Morgans, H. E. G., Handley, L., Pancost, R. D., and Schouten, S.: Middle Eocene climate cyclicity in the southern Pacific: implications for global ice volume, Geology, 36, 651–654, 2008.
Cande, S. C. and Kent, D. V.: Revised calibration of the geomagnetic polarity timescale for the Late Cretaceous and Cenozoic, J. Geophys. Res., 100, 6093–6095, 1995.
Channell, J. E. T., Hodell, D. A., Singer, B. S., and Xuan, C.: Reconciling astrochronological and $^{40}Ar/^{39}Ar$ ages for the Matuyama–Brunhes boundary and late Matuyama Chron, Geochem. Geophy. Geosy., 11, Q0AA12, doi:10.1029/2010GC003203, 2010.
Coxall, H. K. and Wilson, P. A.: Early Oligocene glaciation and productivity in the eastern equatorial Pacific: insights into global carbon cycling, Paleoceanography, 26, PA2221, doi:10.1029/2010pa002021, 2011.
Coxall, H. K., Wilson, P. A., Pälike, H., Lear, C. H., and Backman, J.: Rapid stepwise onset of Antarctic glaciation and deeper calcite compensation in the Pacific Ocean, Nature, 433, 53–57, doi:10.1038/nature03135, 2005.
DeConto, R. M. and Pollard, D.: Rapid Cenozoic glaciation of Antarctica induced by declining atmospheric CO_2, Nature, 421, 245–249, doi:10.1038/nature01290, 2003.
DeConto, R. M., Pollard, D., Wilson, P. A., Pälike, H., Lear, C. H., and Pagani, M.: Thresholds for Cenozoic bipolar glaciation, Nature, 455, 652–656, doi:10.1038/nature07337, 2008.

CPD
9, 6635–6682, 2013

Dunn, D. A.: Change from “Atlantic-type” to “Pacific-type” carbonate stratigraphy in the middle Pliocene Equatorial Pacific Ocean, Mar. Geol., 50, 41–59, doi:10.1016/0025-3227(82)90060-3, 1982.

Dupont-Nivet, G., Krijgsman, W., Langereis, C. G., Abels, H. A., Dai, S., and Fang, X.: Tibetan plateau aridification linked to global cooling at the Eocene–Oligocene transition, Nature, 445, 635–638, doi10.1038/nature05516, 2007.

Edgar, K. M., Wilson, P. A., Sexton, P. F., and Suganuma, Y.: No extreme bipolar glaciation during the main Eocene calcite compensation shift, Nature, 448, 908–911, doi:10.1038/nature06053, 2007.

Ehrmann, W. U. and Mackensen, A.: Sedimentological evidence for the formation of an East Antarctic ice sheet in Eocene/Oligocene time, Palaeogeogr. Palaeocl., 93, 85–112, doi:10.1016/0031-0182(92)90185-8, 1992.

Eldrett, J. S., Harding, I. C., Firth, J. V., and Roberts, A. P.: Magnetostratigraphic calibration of Eocene–Oligocene dinoflagellate cyst biostratigraphy from the Norwegian–Greenland Sea, Mar. Geol., 204, 91–127, 2004.

Eldrett, J. S., Harding, I. C., Wilson, P. A., Butler, E., and Roberts, A. P.: Continental ice in Greenland during the Eocene and Oligocene, Nature, 446, 176–179, doi:10.1038/nature05591, 2007.

Gale, A. S., Huggett, J. M., Pälike, H., Laurie, E., Hailwood, E. A., and Hardenbol, J.: Correlation of Eocene–Oligocene marine and continental records: orbital cyclicity, magnetostratigraphy and sequence stratigraphy of the Solent Group, Isle of Wight, UK, J. Geol. Soc. London, 163, 401–415, doi:10.1144/0016-764903-175, 2006.

Grazzini, C. V. and Oberhaensli, H.: Isotopic Events at the Eocene/Oligocene Transition. A review, in: Developments in Palaeontology and Stratigraphy, edited by: Ch, P. and Premoli-Silva, I., Elsevier, Amsterdam, 311–329, doi:10.1016/S0920-5446(08)70136-5, 1986.

Guidry, E. P., Richter, C., Acton, G. D., Channell, J. E. T., Evans, H. F., Ohneiser, C., Yamamoto, Y., and Yamazaki, T.: Oligocene–Miocene magnetostratigraphy of deep-sea sediments from the Equatorial Pacific (IODP Site U1333), Geol. Soc. London, Spec. Pub., 373, 13–27, doi:10.1144/SP373.7, 2013.

Hilgen, F. J. and Kuiper, K. F.: A critical evaluation of the numerical age of the Eocene–Oligocene boundary, in: The Late Eocene Earth – Hothouse, Icehouse and Impacts, edited by: Koeberl, C. and Montanari, A., Geol. S. Am. S., 139–148, doi:10.1130/2009.2452(09), 2009.

CPD
9, 6635–6682, 2013

Hinnov, L. A. and Hilgen, F. J.: Cyclostratigraphy and astrochronology, in: The Geological Timescale 2012, edited by: Gradstein, F. M., Ogg, J. G., Schmitz, M. D., and Ogg, G. M., Elsevier, Amsterdam, 63–83, doi:10.1016/B978-0-444-59425-9.00004-4, 2012.

Jovane, L., Florindo, F., Sprovieri, M., and Pälike, H.: Astronomic calibration of the late Eocene/early Oligocene Massignano section (central Italy), Geochem. Geophy. Geosy., 7, Q07012, doi:10.1029/2005GC001195, 2006.

Katz, M. E., Cramer, B. S., Toggweiler, J. R., Esmay, G., Liu, C., Miller, K. G., Rosenthal, Y., Wade, B. S., and Wright, J. D.: Impact of Antarctic circumpolar current development on late paleogene ocean structure, Science, 332, 1076–1079, doi:10.1126/science.1202122, 2011.

Kirschvink, J. L.: The least-squares line and plane and the analysis of palaeomagnetic data, Geophys. J. Roy. Astr. S., 62, 699–718, 1980.

Koeberl, C. and Montanari, A. (Eds.) : The Late Eocene Earth – Hothouse, Icehouse and Impacts, Geological Society of America Special Paper, Boulder, Colorado, 322 pp., 2009.

Kuiper, K. F., Deino, A., Hilgen, F. J., Krijgsman, W., Renne, P. R., and Wijbrans, J. R.: Synchronizing rock clocks of Earth history, Science, 320, 500–504, doi:10.1126/science.1154339, 2008.

Kuroda, J., Westerhold, T., and the Expedition 320/321 scientists: Data report: volcanic glass shards from the Eocene–Oligocene transition interval at Site U1333, in: Proc. IODP, 320/321: Tokyo (Integrated Ocean Drilling Program Management International, Inc.), edited by: Pälike, H., Lyle, M., Nishi, H., Raffi, I., Gamage, K., Klaus, A., and the Expedition 320/321 scientists, doi:10.2204/iodp.proc.320321.211.2013, 2013.

Lanci, L., Pares, J. M., Channell, J. E. T., and Kent, D. V.: Miocene magnetostratigraphy from Equatorial Pacific sediments (ODP Site 1218, Leg 199), Earth Planet. Sc. Lett., 226, 207–224, doi:10.1016/j.epsl.2004.07.025, 2004.

Lanci, L., Parés, J. M., Channell, J. E. T., and Kent, D. V.: Oligocene magnetostratigraphy from Equatorial Pacific sediments (ODP Sites 1218 and 1219, Leg 199), Earth Planet. Sc. Lett., 237, 617–634, doi:10.1016/j.epsl.2005.07.004, 2005.

Laskar, J., Joutel, F., and Boudin, F.: Orbital, precessional, and insolation quantities for the Earth from −20 Myr to +10 Myr, Astron. Astrophys., 270, 522–533, 1993.

Laskar, J., Robutel, P., Joutel, F., Gastineau, M., Correia, A., and Levrard, B.: A long-term numerical solution for the insolation quantities of the Earth, Astron. Astrophys., 428, 261–285, doi:10.1051/0004-6361:20041335, 2004.

CPD
9, 6635–6682, 2013

Laskar, J., Fienga, A., Gastineau, M., and Manche, H.: La2010: a new orbital solution for the long-term motion of the Earth, Astron. Astrophys., 532, A89, doi:10.1051/0004-6361/201116836, 2011a.

Laskar, J., Gastineau, M., Delisle, J. B., Farrés, A., and Fienga, A.: Strong chaos induced by close encounters with Ceres and Vesta, Astron. Astrophys., 532, L4, doi:10.1051/0004-6361/201117504, 2011b.

Lear, C. H., Rosenthal, Y., Coxall, H. K., and Wilson, P. A.: Late Eocene to early Miocene ice sheet dynamics and the global carbon cycle, Paleoceanography, 19, PA4015, doi:10.1029/2004PA001039, 2004.

Lear, C. H., Bailey, T. R., Pearson, P. N., Coxall, H. K., and Rosenthal, Y.: Cooling and ice growth across the Eocene–Oligocene transition, Geology, 36, 251–254, 2008.

Leon-Rodriguez, L. and Dickens, G. R.: Data report: stable isotope composition of Eocene bulk carbonate at Sites U1331, U1332, and U1333, in: Proc. IODP, 320/321: Tokyo (Integrated Ocean Drilling Program Management International, Inc.), edited by: Pälike, H., Lyle, M., Nishi, H., Raffi, I., Gamage, K., Klaus, A., and and the Expedition 320/321 scientists, doi:10.2204/iodp.proc.320321.208.2013, 2013.

Liu, Z., Pagani, M., Zinniker, D., DeConto, R., Huber, M., Brinkhuis, H., Shah, S. R., Leckie, R. M., and Pearson, A.: Global cooling during the Eocene–Oligocene climate transition, Science, 323, 1187–1190, doi:10.1126/science.1166368, 2009.

Lourens, L. J., Sluijs, A., Kroon, D., Zachos, J. C., Thomas, E., Röhl, U., Bowles, J., and Raffi, I.: Astronomical pacing of late Palaeocene to early Eocene global warming events, Nature, 435, 1083–1087, doi:10.1038/nature03814, 2005.

Lowrie, W. and Lanci, L.: Magnetostratigraphy of Eocene–Oligocene boundary sections in Italy: no evidence for short subchrons within chrons 12R and 13R, Earth Planet. Sc. Lett., 126, 247–258, doi:10.1016/0012-821X(94)90110-4, 1994.

Lyle, M. W., Wilson, P. A., Janecek, T. R., Backman, J., Busch, W. H., Coxall, H. K., Faul, K., Gaillot, P., Hovan, S. A., Knoop, P., Kruse, S., Lanci, L., Lear, C., Moore, T. C., Nigrini, C. A., Nishi, H., Nomura, R., Norris, R. D., Pälike, H., Parés, J. M., Quintin, L., Raffi, I., Rea, B. R., Rea, D. K., Steiger, T. H., Tripati, A., Vanden Berg, M. D., and Wade, B.: Proc. ODP, Init. Repts., 199: College Station, TX (Ocean Drilling Program), 2002.

Miller, K. G., Wright, J. D., and Fairbanks, R. G.: Unlocking the icehouse: Oligocene-Miocene oxygen isotope, eustacy, and margin erosion, J. Geophys. Res., 96, 6829–6848, 1991.

CPD
9, 6635–6682, 2013

Moore Jr., T. C.: Erosion and reworking of Pacific sediments near the Eocene-Oligocene boundary, Paleoceanography, 28, 263–273, doi:10.1002/palo.20027, 2013.
Moore Jr., T. C., Pisias, N. G., and Dunn, D. A.: Carbonate time series of the Quaternary and Late Miocene sediments in the Pacific Ocean: a spectral comparison, Mar. Geol., 46, 217–233, doi:10.1016/0025-3227(82)90081-0, 1982.
Ogg, J. G.: Geomagnetic polarity time scale, in: The Geological Timescale 2012, edited by: Gradstein, F., Ogg, J., Schmitz, M. D., and Ogg, G. M., Elsevier, Amsterdam, 85–114, 2012.
Ogg, J. G. and Smith, A. G.: The geomagnetic polarity time scale, in: A Geological Timescale 2004, edited by: Gradstein, F., Ogg, J., and Smith, A., Cambridge University Press, Cambridge, 63–86, 2004.
Pälike, H., Shackleton, N. J., and Röhl, U.: Astronomical forcing in Late Eocene marine sediments, Earth Planet. Sc. Lett., 193, 589–602, 2001.
Pälike, H., Nishi, H., Lyle, M., Raffi, I., Gamage, K., Klaus, A., and the Expedition 320/321 scientists: Proc. IODP, 320/321: Tokyo (Integrated Ocean Drilling Program Management International, Inc.), 2010. 2002.
Pälike, H., Moore, T., Backman, J., Raffi, I., Lanci, L., Parés, J. M., and Janecek, T.: Integrated stratigraphic correlation and improved composite depth scales for ODP Sites 1218 and 1219, in: Proc. ODP, Sci. Results, 199: College Station, TX (Ocean Drilling Program), edited by: Wilson, P. A., Lyle, M., and Firth, J. V., 1–41, doi:10.2973/odp.proc.sr.199.213.2005, 2005.
Pälike, H., Norris, R. D., Herrle, J. O., Wilson, P. A., Coxall, H. K., Lear, C. H., Shackleton, N. J., Tripati, A. K., and Wade, B. S.: The heartbeat of the Oligocene climate system, Science, 314, 1894–1898, doi:10.1126/science.1133822, 2006.
Pälike, H., Lyle, M. W., Nishi, H., Raffi, I., Ridgwell, A., Gamage, K., Klaus, A., Acton, G., Anderson, L., Backman, J., Baldauf, J., Beltran, C., Bohaty, S. M., Bown, P., Busch, W., Channell, J. E. T., Chun, C. O. J., Delaney, M., Dewangan, P., Dunkley Jones, T., Edgar, K. M., Evans, H., Fitch, P., Foster, G. L., Gussone, N., Hasegawa, H., Hathorne, E. C., Hayashi, H., Herrle, J. O., Holbourn, A., Hovan, S., Hyeong, K., Iijima, K., Ito, T., Kamikuri, S.-i., Kimoto, K., Kuroda, J., Leon-Rodriguez, L., Malinverno, A., Moore Jr., T. C., Murphy, B. H., Murphy, D. P., Nakamura, H., Ogane, K., Ohneiser, C., Richter, C., Robinson, R., Rohling, E. J., Romero, O., Sawada, K., Scher, H., Schneider, L., Sluijs, A., Takata, H., Tian, J., Tsujimoto, A., Wade, B. S., Westerhold, T., Wilkens, R., Williams, T., Wilson, P. A., Yamamoto, Y., Yamamoto, S., Yamazaki, T., and Zeebe, R. E.: A Cenozoic record of the equatorial Pacific carbonate compensation depth, Nature, 488, 609–614, doi:10.1038/nature11360, 2012.

CPD
9, 6635–6682, 2013

Pearson, P. N. and Palmer, M. R.: Atmospheric carbon dioxide concentrations over the past 60 million years, Nature, 406, 695–699, doi:10.1038/35021000, 2000.
Pearson, P. N., van Dongen, B. E., Nicholas, C. J., Pancost, R. D., Schouten, S., Singano, J. M., and Wade, B. S.: Stable warm tropical climate through the Eocene Epoch, Geology, 35, 211–214, doi:10.1130/g23175a.1, 2007.
Peters, S. E., Carlson, A. E., Kelly, D. C., and Gingerich, P. D.: Large-scale glaciation and deglaciation of Antarctica during the Late Eocene, Geology, 38, 723–726, doi:10.1130/g31068.1, 2010.
Pollard, D. and DeConto, R. M.: Hysteresis in Cenozoic Antarctic ice-sheet variations, Global Planet. Change, 45, 9–21, doi:10.1016/j.gloplacha.2004.09.011, 2005.
Premoli Silva, I. and Jenkins, G. D.: Decision on the Eocene–Oligocene boundary stratotype, Episodes, 16, 379–382, 1993.
Prentice, M. L. and Matthews, R. K.: Cenozoic ice-volume history: development of a composite oxygen isotope record, Geology, 16, 963–966, doi:10.1130/0091-7613(1988)016<0963:civhdo>2.3.co;2, 1988.
Prothero, D. R. and Emry, R. J.: The Terrestrial Eocene–Oligocene Transition in North America, Cambridge University Press, Cambridge, 1996.
Prothero, D. R., Ivany, L. C., and Nesbitt, E. A.: From Greenhouse to Icehouse: the Marine Eocene–Oligocene Transition, Columbia University Press, New York, 2003.
Röhl, U. and Abrams, L. J.: High-resolution, downhole and non-destructive core measurements from Sites 999 and 1001 in the Caribbean Sea: application to the Late Paleocene Thermal Maximum, in: Proc. ODP, Sci. Results, 165, edited by: Leckie, R. M., Sigurdsson, H., Acton, G. D., and Draper, G., 191–203, 2000.
Röhl, U., Wefer, G., Brinkhuis, H., Stickley, C. E., Fuller, M., Schellenberg, S. A., and Williams, G. L.: Sea level and astronomically induced environmental changes in middle and late sediments from the East Tasman Plateau, in: The Cenozoic Southern Ocean: Tectonics, Sedimentation and Climate Change between Australia and Antarctica, edited by: Exon, N. F., Kennett, J. P., and Malone, M. J., Am. Geophys. Union, Geophys. Monogr., 151, 113–126, 2004.
Röhl, U., Westerhold, T., Bralower, T. J., and Zachos, J. C.: On the duration of the Paleocene–Eocene thermal maximum (PETM), Geochem. Geophy. Geosy., 8, Q12002, doi:10.1029/2007GC001784, 2007.

CPD
9, 6635–6682, 2013

Shackleton, N. J. and Kennett, J. P.: Paleotemperature history of the Cenozoic and the initiation of Antarctic glaciation: oxygen and carbon isotope analyses in DSDP Sites 277, 279, and 281, in: Init. Repts. DSDP, 29, edited by: Kennett, J. P., Houtz, R. E., and et al., US Govt. Printing Office, Washington, 743–755, 1975.

Sloan, L. C. and Huber, M.: Eocene oceanic responses to orbital forcing on precessional time scales, Paleoceanography, 16, 101–111, doi:10.1029/1999pa000491, 2001.

Smith, M. E., Chamberlain, K. R., Singer, B. S., and Carroll, A. R.: Eocene clocks agree: Coeval $^{40}Ar/^{39}Ar$, U-Pb, and astronomical ages from the Green River Formation, Geology, 38, 527–530, doi:10.1130/g30630.1, 2010.

Stickley, C. E., St John, K., Koc, N., Jordan, R. W., Passchier, S., Pearce, R. B., and Kearns, L. E.: Evidence for middle Eocene Arctic sea ice from diatoms and ice-rafted debris, Nature, 460, 376–379, doi:10.1038/nature08163, 2009.

St. John, K.: Cenozoic ice-rafting history of the central Arctic Ocean: terrigenous sands on the Lomonosov Ridge, Paleoceanography, 23, PA1S05, doi:10.1029/2007PA001483, 2008.

Tripati, A., Backman, J., Elderfield, H., and Ferretti, P.: Eocene bipolar glaciation associated with global carbon cycle changes, Nature, 436, 341–346, doi:10.1038/nature03874, 2005.

Tripati, A. K., Eagle, R. A., Morton, A., Dowdeswell, J. A., Atkinson, K. L., Bahe, Y., Dawber, C. F., Khadun, E., Shaw, R. M. H., Shorttle, O., and Thanabalasundaram, L.: Evidence for glaciation in the Northern Hemisphere back to 44 Ma from ice-rafted debris in the Greenland Sea, Earth Planet. Sc. Lett., 265, 112–122, 2008.

Van Andel, T. H.: Mesozoic/cenozoic calcite compensation depth and the global distribution of calcareous sediments, Earth Planet. Sc. Lett., 26, 187–194, doi:10.1016/0012-821x(75)90086-2, 1975.

Vandenberghe, N., Hilgen, F. J., and Speijer, R. P.: The paleogene period, in: The Geological Timescale 2012, edited by: Gradstein, F. M., Ogg, J. G., Schmitz, M. D., and Ogg, G. M., Elsevier, Amsterdam, 855–922, doi:10.1016/B978-0-444-59425-9.00028-7, 2012.

Vonhof, H. B., Smit, J., Brinkhuis, H., Montanari, A., and Nederbragt, A. J.: Global cooling accelerated by early late Eocene impacts?, Geology, 28, 687–690, doi:10.1130/0091-7613(2000)28<687:gcabel>2.0.co;2, 2000.

Wade, B. S. and Pälike, H.: Oligocene climate dynamics, Paleoceanography, 19, PA4019, doi:10.1029/2004PA001042, 2004.

Walsh, S. L., Prothero, D. R., and Lundquist, D. J.: Stratigraphy and paleomagnetism of the middle Eocene Friars Formation and Poway Group, southwestern San Diego County,

CPD
9, 6635–6682, 2013

California, in: The Terrestrial Eocene–Oligocene Transition in North America, edited by: Prothero, D. R. and Emry, R. J., Cambridge University Press, Cambridge, 120–151, doi:10.1017/CBO9780511665431.007, 1996.
Westerhold, T. and Röhl, U.: High resolution cyclostratigraphy of the early Eocene – new insights into the origin of the Cenozoic cooling trend, Clim. Past, 5, 309–327, doi:10.5194/cp-5-309-2009, 2009.
Westerhold, T., and Röhl, U.: Orbital pacing of Eocene climate during the Middle Eocene Climate Optimum and the chron C19r event: Missing link found in the tropical western Atlantic, Geochem. Geophys. Geosyst., 14, 4811–4825, doi:10.1002/ggge.20293, 2013.
Westerhold, T., Röhl, U., Laskar, J., Bowles, J., Raffi, I., Lourens, L. J., and Zachos, J. C.: On the duration of magnetochrons C24r and C25n and the timing of early Eocene global warming events: implications from the Ocean Drilling Program Leg 208 Walvis Ridge depth transect, Paleoceanography, 22, PA2201, doi:10.1029/2006PA001322, 2007.
Westerhold, T., Röhl, U., Donner, B., McCarren, H. K., and Zachos, J. C.: A complete high-resolution Paleocene benthic stable isotope record for the central Pacific (ODP Site 1209), Paleoceanography, 26, Pa2216, doi:10.1029/2010pa002092, 2011.
Westerhold, T., Röhl, U., Wilkens, R., Pälike, H., Lyle, M., Jones, T. D., Bown, P., Moore, T., Kamikuri, S., Acton, G., Ohneiser, C., Yamamoto, Y., Richter, C., Fitch, P., Scher, H., Liebrand, D., and the Expedition 320/321 scientists: Revised composite depth scales and integration of IODP Sites U1331-U1334 and ODP Sites 1218–1220, in: Proc. IODP, 320/321: Tokyo (Integrated Ocean Drilling Program Management International, Inc.), edited by: Pälike, H., Lyle, M., Nishi, H., Raffi, I., Gamage, K., Klaus, A., and the Expedition 320/321 scientists, doi:10.2204/iodp.proc.320321.201.2012, 2012a.
Westerhold, T., Röhl, U., and Laskar, J.: Time scale controversy: accurate orbital calibration of the early Paleogene, Geochem. Geophy. Geosy., 13, Q06015, doi:10.1029/2012gc004096, 2012b.
Wilkens, R., Dickens, G. R., Tian, J., Backman, J., and the Expedition 320/321 scientists: Data report: revised composite depth scales for Sites U1336, U1337, and U1338, in: Proc. IODP, 320/321: Tokyo (Integrated Ocean Drilling Program Management International, Inc.), edited by: Pälike, H., Lyle, M., Nishi, H., Raffi, I., Gamage, K., Klaus, A., and the Expedition 320/321 scientists, doi:10.2204/iodp.proc.320321.201.2012, 2013.
Xiao, G. Q., Abels, H. A., Yao, Z. Q., Dupont-Nivet, G., and Hilgen, F. J.: Asian aridification linked to the first step of the Eocene-Oligocene climate Transition (EOT) in obliquity-dominated

CPD
9, 6635–6682, 2013

terrestrial records (Xining Basin, China), Clim. Past, 6, 501–513, doi:10.5194/cp-6-501-2010, 2010.
Zachos, J. C., Stott, L. D., and Lohmann, K. C.: Evolution of early Cenozoic marine temperatures, Paleoceanography, 9, 353–387, doi:10.1029/93PA03266, 1994.
Zachos, J. C., Quinn, T. M., and Salamy, K. A.: High-resolution (10^4 years) deep-sea foraminiferal stable isotope records of the Eocene–Oligocene climate transition, Paleoceanography, 11, 251–266, doi:10.1029/96PA00571, 1996.
Zachos, J., Pagani, M., Sloan, L., Thomas, E., and Billups, K.: Trends, rhythms, and aberrations in global climate 65 Ma to present, Science, 292, 686–693, doi:10.1126/science.1059412, 2001.
Zachos, J. C., McCarren, H., Murphy, B., Röhl, U., and Westerhold, T.: Tempo and scale of late Paleocene and early Eocene carbon isotope cycles: implications for the origin of hyperthermals, Earth Planet. Sc. Lett., 299, 242–249, doi:10.1016/j.epsl.2010.09.004, 2010.

CPD
9, 6635–6682, 2013

Table 1. Comparison of magnetochron boundary ages in million years.

Chron	Standard GPTS			Tuned – this study[a]		Tuned						
	CK95	GPTS 2004	GPTS 2012	PEAT Sites[b]	ODP Site 1052	ODP Site 1260	Pälike et al. (2006)	Pälike et al. (2001)	Gale et al. (2006)	Hyland et al. (2009)	Jovane et al. (2006)	Jovane et al. (2010)
C12n (o)	30.939	31.116	31.034	30.977 ± 16			31.021			31.600		
C13n (y)	33.058	33.266	33.157	33.214 ± 2			33.232		33.503	33.230		
C13n (o)	33.545	33.738	33.705	33.726 ± 8			33.705		33.626	33.750		
C13r.14	33.7	33.9	33.9	33.890			33.79			33.95	33.714	
C15n (y)	34.655	34.782	34.999	35.102 ± 32			35.126		34.621		34.640	
C15n (o)	34.940	35.043	35.294	35.336 ± 17			35.254		34.988		34.960	
C16n.1n (y)	35.343	35.404	35.706	35.580 ± 15			35.328	35.185			35.343	
C16n.1n (o)	35.526	35.567	35.892	35.718 ± 22	35.735 ± 32		35.554	35.524				
C16n.2n (y)	35.685	35.707	36.051	35.774 ± 21	35.817 ± 36		35.643	35.605				
C16n.2n (o)	36.341	36.276	36.700	36.351 ± 6	36.264 ± 78		36.355	36.051				
C17n.1n (y)	36.618	36.512	36.969	36.573 ± 5	36.574 ± 40		36.668	36.404				
C17n.1n (o)	37.473	37.235	37.753	37.385 ± 7	37.445 ± 42		37.520	37.300				
C17n.2n (y)	37.604	37.345	37.872	37.530 ± 3	37.559 ± 24		37.656	37.399				
C17n.2n (o)	37.848	37.549	38.093	37.781 ± 7	37.742 ± 26		37.907	37.618				
C17n.3n (y)	37.920	37.610	38.159	37.858 ± 7	37.824 ± 22		37.956	37.692				
C17n.3n (o)	38.113	37.771	38.333	38.081 ± 11	38.054 ± 42		38.159	37.897				
C18n.1n (y)	38.426	38.032	38.615	38.398 ± 7	38.370 ± 38		38.449	38.186				
C18n.1n (o)	39.552	38.975	39.627	39.582 ± 4			39.554	39.441				
C18n.2n (y)	39.631	39.041	39.698	39.666 ± 3			39.602	39.486				
C18n.2n (o)	40.130	39.464	40.145	40.073 ± 1			40.084	39.828				40.120
C19n (y)	41.257	40.439	41.154	*41.072 ± 2*		41.061 ± 9	41.358					41.250
C19n (o)	41.521	40.671	41.390	*41.306 ± 4*		41.261 ± 4	41.510					41.510
C20n (y)	42.536	41.590	42.301			42.151 ± 7						42.540

[a] Tuned to the orbital solution La2011 (Laskar et al., 2011).
[b] Combined ages based on Pacific Equatorial Age Transect Sites 1218, U1333 and U1334.

CPD
9, 6635–6682, 2013

Table 2. Comparison of magnetochron boundary durations in million years.

Chron	Standard GPTS			Tuned – this study[a]		Tuned						
	CK95	GPTS 2004	GPTS 2012	PEAT Sites[b]	ODP Site 1052	ODP Site 1260	Pälike et al. (2006)	Pälike et al. (2001)	Gale et al. (2006)	Hyland et al. (2009)	Jovane et al. (2006)	Jovane et al. (2010)
C12r	2.119	2.150	2.123	2.237 ± 18			2.211			1.630		
C13n	0.487	0.472	0.548	0.512 ± 10			0.473		0.123	0.520		
C13r	1.110	1.044	1.294	1.376 ± 41			1.421		0.995			
C15n	0.285	0.260	0.295	0.234 ± 49			0.128		0.367		0.320	
C15r	0.403	0.361	0.412	0.245 ± 31			0.074				0.383	
C16n.1n	0.183	0.163	0.186	0.138 ± 36			0.226	0.339				
C16n.1r	0.159	0.140	0.159	0.056 ± 42	0.082 ± 68		0.089	0.081				
C16n.2n	0.656	0.569	0.649	0.577 ± 27	0.447 ± 114		0.712	0.446				
C16n.2r	0.277	0.237	0.269	0.222 ± 11	0.310 ± 118		0.313	0.353				
C17n.1n	0.855	0.723	0.784	0.811 ± 12	0.871 ± 82		0.852	0.896				
C17n.1r	0.131	0.110	0.119	0.146 ± 10	0.114 ± 66		0.136	0.099				
C17n.2n	0.244	0.204	0.221	0.251 ± 10	0.183 ± 50		0.251	0.219				
C17n.2r	0.072	0.060	0.066	0.077 ± 14	0.082 ± 48		0.049	0.074				
C17n.3n	0.193	0.161	0.174	0.223 ± 17	0.230 ± 64		0.203	0.205				
C17n.3r	0.313	0.261	0.282	0.317 ± 18	0.316 ± 80		0.290	0.289				
C18n.1n	1.126	0.943	1.012	1.184 ± 12			1.105	1.255				
C18n.1r	0.079	0.066	0.071	0.083 ± 7			0.048	0.045				
C18n.2n	0.499	0.424	0.447	0.407 ± 4			0.482	0.342				
C18n.2r	1.127	0.975	1.009	0.999 ± 4			1.274					1.130
C19n	0.264	0.232	0.236	*0.236 ± 6*		0.200 ± 18	0.152					0.260
C19r	1.015	0.918	0.911	*0.845 ± 7*		0.890 ± 18	1.026					1.030

[a] Tuned to the orbital solution La2011 (Laskar et al., 2011).
[b] Duration based on Pacific Equatorial Age Transect Sites 1218, U1333 and U1334.

CPD
9, 6635–6682, 2013

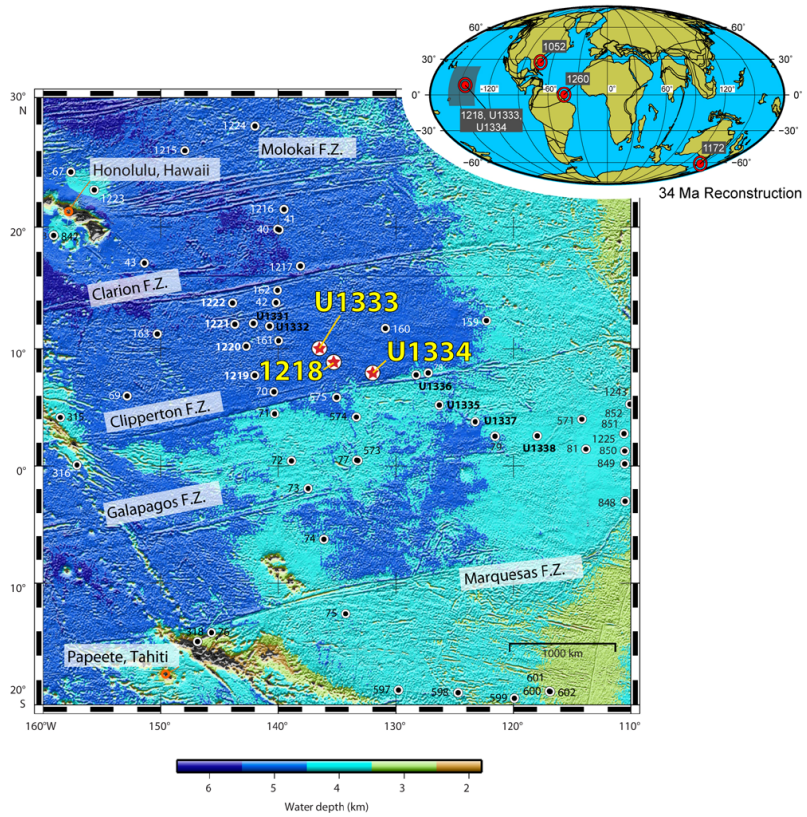

Fig. 1. Location map of sites used in this study on 34 Ma paleogeographic reconstruction in Mollweide projection (http://www.odsn.de, Hay et al., 1999) and detailed location map in the Pacific (big map, red stars) with additional IODP/ODP/DSDP sites. F.Z. = fracture zone (modified from Pälike et al., 2010).

CPD
9, 6635–6682, 2013

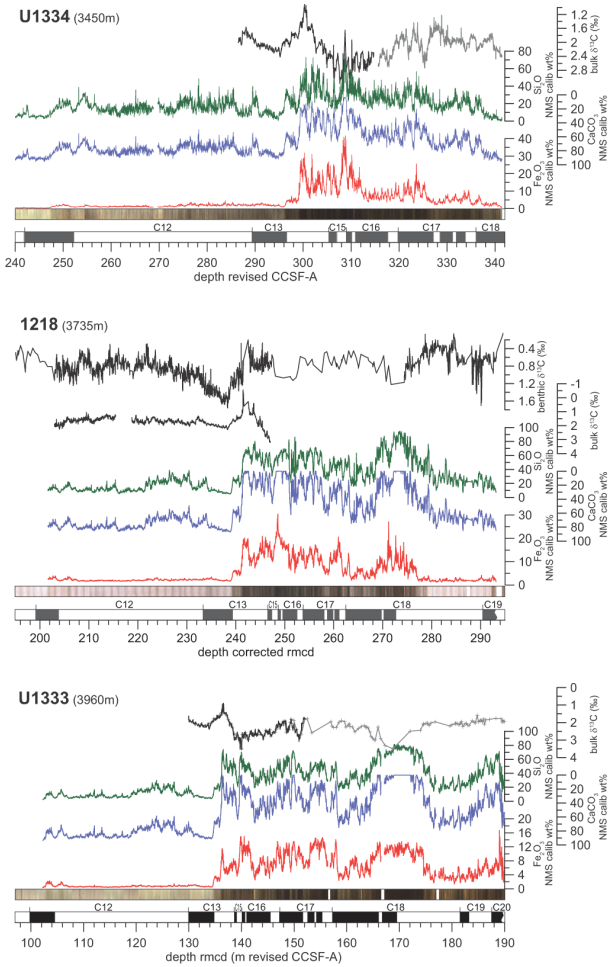

CPD
9, 6635–6682, 2013

Orbitally tuned time scale and astronomical forcing

T. Westerhold et al.

Fig. 2. Overview of data from ODP Site 1218 and IODP Sites U1333/U1334 in the depth domain (in brackets the water depth of each site at 34 Ma; Pälike et al., 2010). The plots show stable carbon isotope data (black, gray), Normalized Median Scaled (NMS) wt % based on calibrated XRF core scanning data for Si (green), Ca (blue), and Fe (red) (for details see methods chapter), spliced core image, and magnetic polarity reversal pattern transferred to 1218 and U1334 by correlation to U1333 (Pälike et al., 2010; Westerhold et al., 2012a). Data sources: all XRF core scanning data from this study; bulk δ^{13}C U1334 from Wilson et al. (unpublished) (black) and this study (gray), 1218 from Coxall et al. (2005) (black), U1333 from Wilson et al. (unpublished) (black) and Léon-Rodriguez and Dickens (2013) (gray); benthic (*Cibicidoides* spp.) δ^{13}C of 1218 from Lear et al. (2004), Coxall et al. (2005), Tripati et al. (2005), and Coxall and Wilson (2011).

CPD
9, 6635–6682, 2013

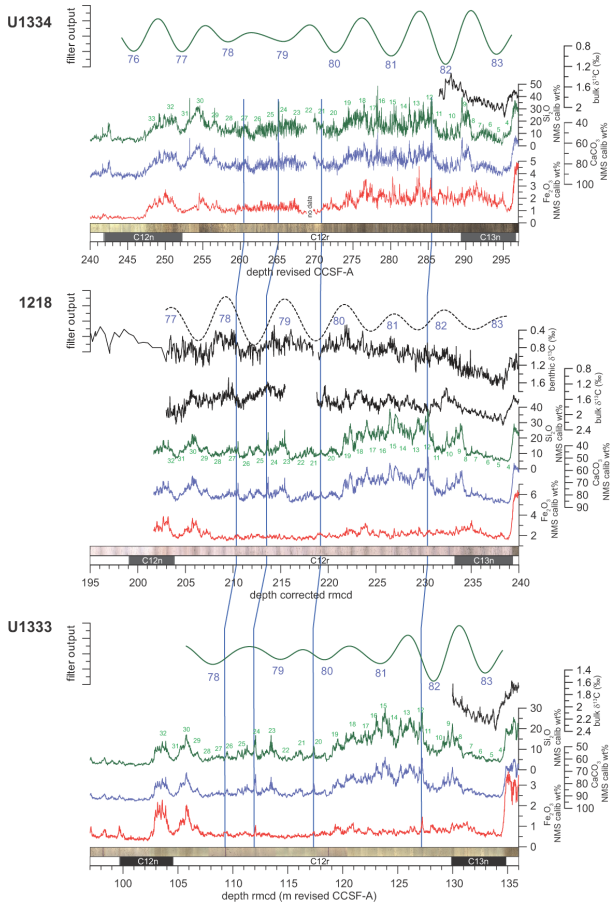

CPD
9, 6635–6682, 2013

Orbitally tuned time scale and astronomical forcing

T. Westerhold et al.

Fig. 3. High-resolution XRF core scanning data, bulk and benthic stable carbon isotope data, core images and cyclostratigraphy from Chron C12n to C13n for Sites U1334, 1218, and U1333 in the depth domain. For details see captions of Fig. 2. Blue lines mark early Oligocene ash layers apparent in all three sites (Kuroda and Westerhold, 2013). Numbers represent the assigned short (green) and long (blue) eccentricity cycle maxima positions in the orbital solution (see Supplement Fig. S8). Band pass filters: for Site U1334 from Si data ($0.14 \pm 0.042\,\mathrm{cm}^{-1}$ ($\mathrm{cycle\,m}^{-1}$); 7.2 m band in Supplement Fig. S2a); for Site 1218 from benthic stable carbon isotope data ($0.164 \pm 0.049\,\mathrm{cm}^{-1}$); for Site U1333 from Si data ($0.2 \pm 0.06\,\mathrm{cm}^{-1}$; 5 m band in Supplement Fig. S2c).

CPD
9, 6635–6682, 2013

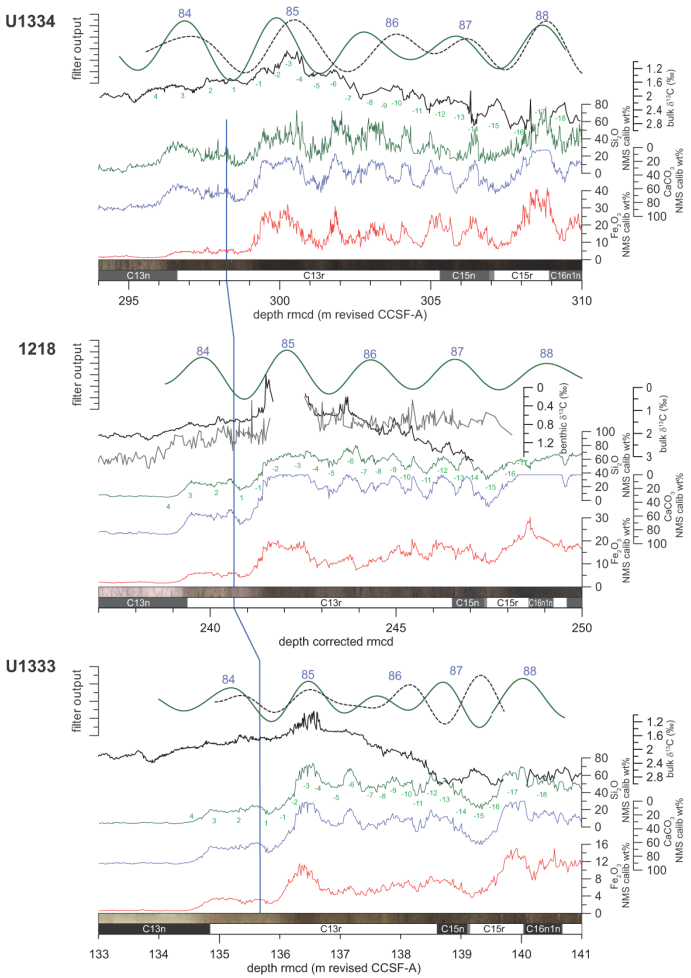

CPD
9, 6635–6682, 2013

Orbitally tuned time scale and astronomical forcing

T. Westerhold et al.

Fig. 4. High-resolution XRF core scanning data, bulk and benthic stable carbon isotope data, core images and cyclostratigraphy from Chron C13n to C15r for Sites U1334, 1218 and U1333 in the depth domain. For details see caption of Fig. 2. 405 kyr band pass filters: for Site U1334 from Si data (green line; $0.34 \pm 0.102\,cm^{-1}$; 2.95 m band in Supplement Fig. S5a) and bulk stable carbon isotopes (dashed black line; $0.33 \pm 0.099\,cm^{-1}$; 3.03 m band in Supplement Fig. S1a); for Site 1218 from Si data ($0.42 \pm 0.126\,cm^{-1}$; 2.38 m band in Supplement Fig. S5b); for Site U1333 from Si data (green, $0.82 \pm 0.25\,cm^{-1}$; 1.22 m band in Supplement Fig. S5c) and bulk stable carbon isotopes (dashed black line; $0.82 \pm 0.25\,cm^{-1}$; 1.22 m band in Supplement Fig. S1b).

CPD
9, 6635–6682, 2013

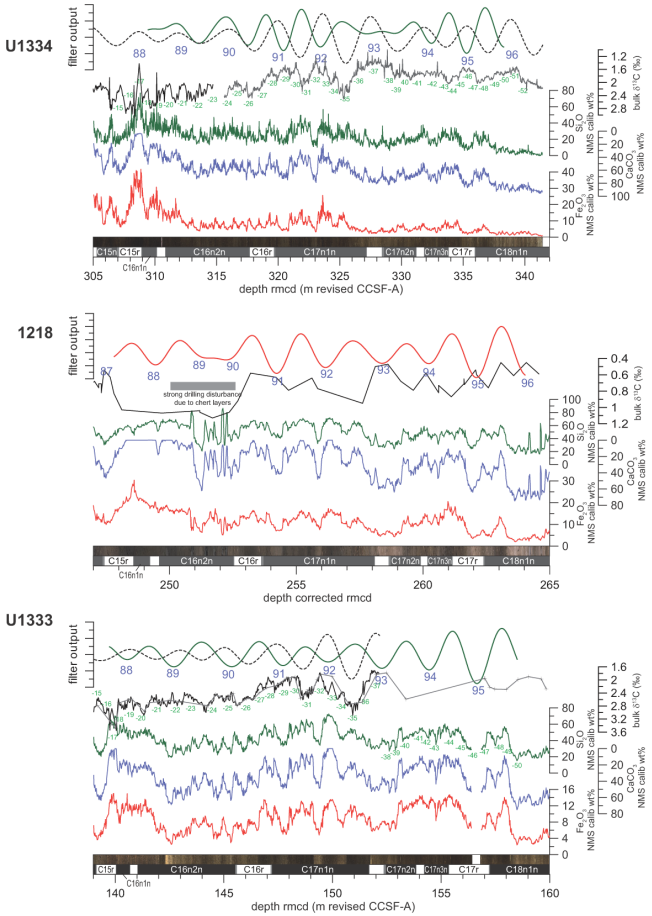

CPD
9, 6635–6682, 2013

Orbitally tuned time scale and astronomical forcing

T. Westerhold et al.

Fig. 5. High-resolution XRF core scanning data, bulk and benthic stable carbon isotope data, core images and cyclostratigraphy from Chron C15r to C18n.1n for Sites U1334, 1218, and U1333 in the depth domain. For details see caption of Fig. 2. 405 kyr band pass filters: for Site U1334 from Si data (green line; $0.26 \pm 0.075\,\mathrm{cm}^{-1}$; 3.85 m band in Supplement Fig. S5a) and bulk stable carbon isotopes (dashed black line; $0.26 \pm 0.075\,\mathrm{cm}^{-1}$; 3.85 m band in Supplement Fig. S1a); for Site 1218 from Fe data ($0.48 \pm 0.14\,\mathrm{cm}^{-1}$; 2.08 m band in Supplement Fig. S6b); for Site U1333 from Si data (green, $0.43 \pm 0.13\,\mathrm{cm}^{-1}$; 2.33 m band in Supplement Fig. S5c) and bulk stable carbon isotopes (dashed black line; $0.43 \pm 0.13\,\mathrm{cm}^{-1}$; 2.33 m band in Supplement Fig. S1b).

CPD
9, 6635–6682, 2013

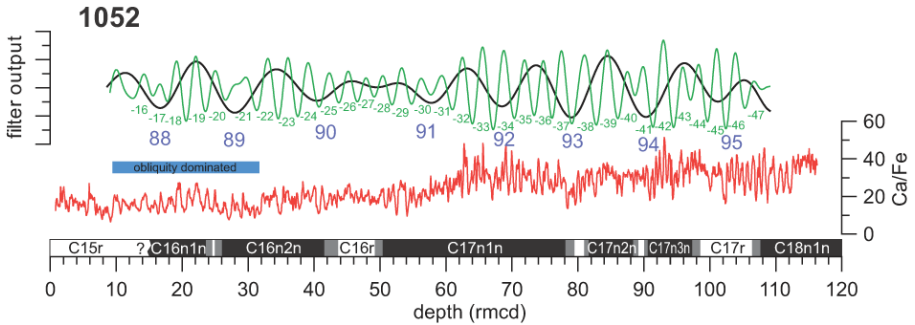

Fig. 6. Cyclostratigraphy from Chron C15r to C18n.1n for ODP Site 1052 in the depth domain. Ca/Fe data and paleomagnetic reversal pattern from Pälike et al. (2001). Numbers represent the assigned short (green) and long (blue) eccentricity cycle maxima positions in the orbital solution (see Supplement Fig. S8). Band pass filters: 405 kyr filter in black ($0.09 \pm 0.027\,\mathrm{cm}^{-1}$); 100 kyr filter in green ($0.32 \pm 0.096\ \mathrm{cm}^{-1}$). Please note the strong obliquity component present from 10 to 30 rmcd in the 1052 sedimentary record.

CPD
9, 6635–6682, 2013

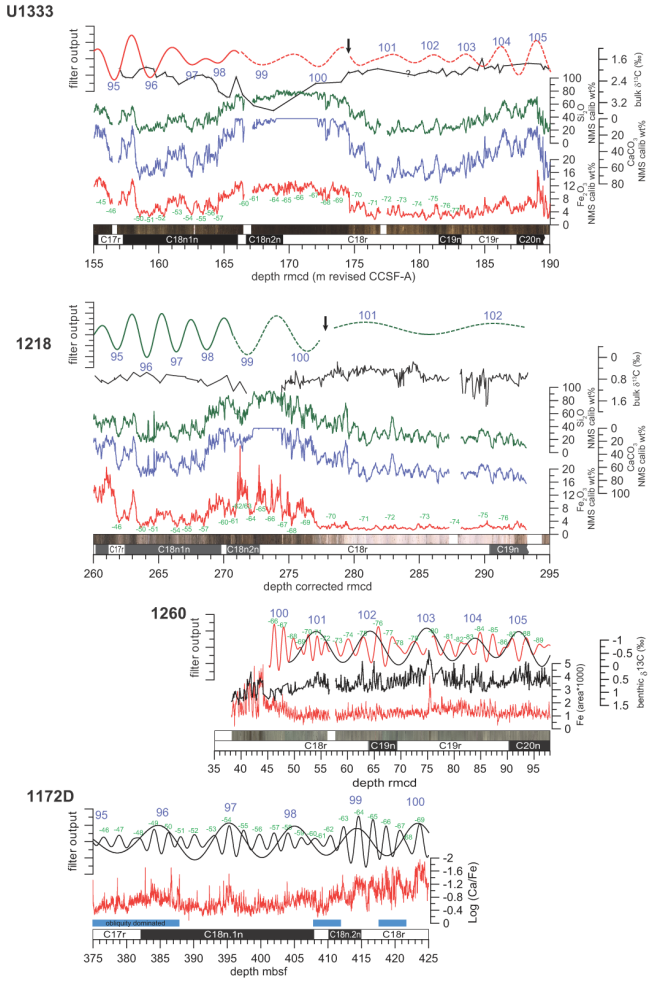

CPD
9, 6635–6682, 2013

Orbitally tuned time scale and astronomical forcing

T. Westerhold et al.

Fig. 7. High-resolution XRF core scanning data, bulk and benthic stable carbon isotope data, core images and cyclostratigraphy from Chron C18n.1n to C20n for Sites U1333, 1218, 1260 and Hole 1172D in the depth domain. For details see caption of Fig. 2. ODP Site 1260 XRF Fe intensity data from Westerhold and Röhl (2013) and benthic stable isotope data from Edgar et al. (2007). ODP 1172D data from Röhl et al. (2004). Arrows mark change in phase relation between stable isotope and XRF core scanning data. 405 kyr band pass filters: for Site U1333 from Fe data (155 to 165 rmcd $0.36 \pm 0.110\,\mathrm{cm}^{-1}$; 165 to 175 rmcd $0.25 \pm 0.07\,\mathrm{cm}^{-1}$; 175 to 190 rmcd $0.36 \pm 0.1\,\mathrm{cm}^{-1}$; 2.78 m, 4 m, 2.78 m bands in Supplement Fig. S6c); for Site 1218 from Si data (260 to 270 rmcd $0.42 \pm 0.105\,\mathrm{cm}^{-1}$; 270 to 278 rmcd $0.22 \pm 0.05\,\mathrm{cm}^{-1}$; 278 to 293 rmcd $0.11 \pm 0.027\,\mathrm{cm}^{-1}$; 2.38 m, 4.55 m, 9.09 m bands in Supplement Fig. S5b); for Site 1260 from benthic stable carbon isotope data ($0.1 \pm 0.03\,\mathrm{cm}^{-1}$); for Hole 1172D from log(Ca/Fe) data ($0.1 \pm 0.03\,\mathrm{cm}^{-1}$). Note the dominant obliquity component in Hole 1172D.

CPD
9, 6635–6682, 2013

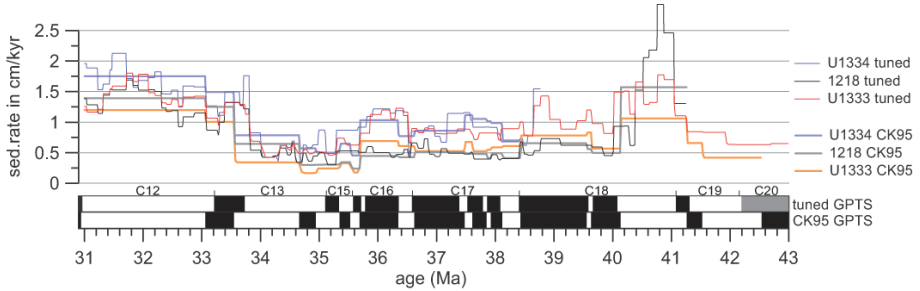

Fig. 8. Sedimentation rate estimate in cm kyr^{-1} based on astronomical tuning compared with paleomagnetic based estimates using the time scale of Cande and Kent (1995, CK95). For reference the CK95 and tuned GPTS (this study) are drawn.

CPD
9, 6635–6682, 2013

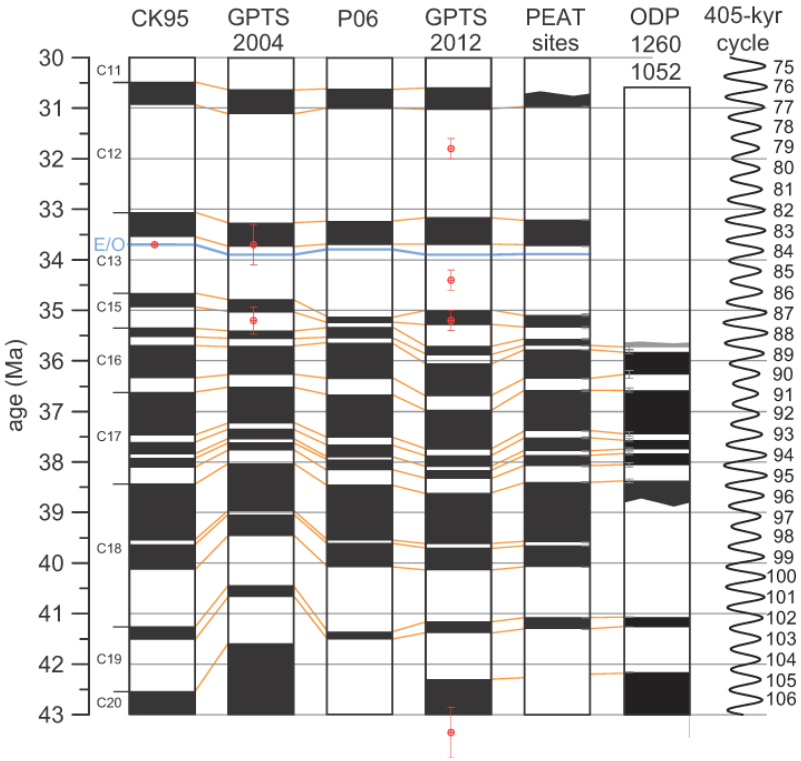

Fig. 9. Comparison of magnetochron boundary ages and durations for Chron C12 to C19 based on estimates from Cande and Kent (1995; CK95), Ogg and Smith (2004; GPTS 2004), Pälike et al. (2006; P06), Ogg (2012; GPTS 2012), Pacific Equatorial Age Transect (PEAT; this study), and combined ODP Sites 1052 and 1260 (this study). Orange lines track changes between different estimates. Calibration points with error bar used by CK95, GPTS2004 and GPTS2012 are plotted in red dots. Also given is the respective absolute age of the Eocene/Oligocene boundary (E/O; blue line) and the long eccentricity cycle number for reference (see Supplement Fig. S8).

CPD
9, 6635–6682, 2013

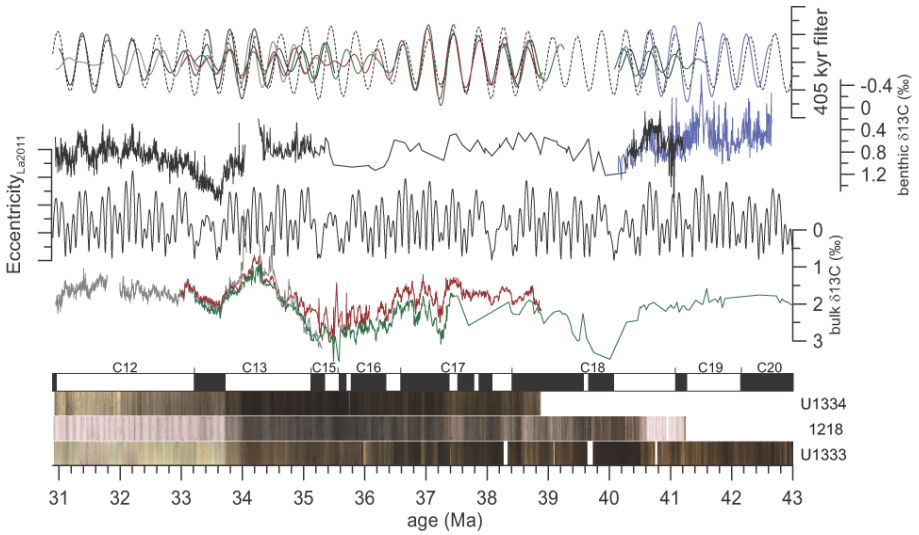

Fig. 10. Tuned bulk and benthic stable carbon isotope data plotted against La2011 orbital solution for eccentricity (Laskar et al., 2011). Bulk data: 1218 (gray; Pälike et al., 2006), U1333 (green; this paper; Wilson et al., unpublished; Leon-Rodriquez and Dickens, 2013), U1334 (red; this paper; Wilson et al., unpublished). Benthic data: 1218 (black; Lear et al., 2004; Coxall et al., 2005; Tripati et al., 2005; Coxall and Wilson, 2011), 1260 (blue; Edgar et al., 2007). Long eccentricity (405 kyr) band pass filters of the detrended, tuned records are plotted on top La2011 (dash line). Magnetostratigraphy as provided in Table 1 and combined core images from Site U1333, U1334, and 1218 for illustration.

CPD
9, 6635–6682, 2013